Piezo1 knockdown alleviates high-altitude cerebral edema by improving brain microvascular endothelial cell tight junctions via blocking the calcium influx-mediated Calpain-1 activity

TAIJIAN CAO[1], ZHICHENG XIANG[2], YANGYANG ZHAO[3], DROLMA GOMCHOK[2], HAIFENG MA[4], SHIWANG LI[2], DAHAI CAO[2], CHUNQING YANG[2] and QIANG ZHANG[5]

[1]Department of Spinal Surgery, Qinghai University Affiliated Hospital, College of Clinical Medicine, Qinghai University, Xining, Qinghai 810001, P.R. China; [2]College of Clinical Medicine, Qinghai University, Xining, Qinghai 810001, P.R. China; [3]Department of Dermatology and Plastic Surgery, Qinghai University Affiliated Hospital, College of Clinical Medicine, Qinghai University, Xining, Qinghai 810001, P.R. China; [4]Department of Neurosurgery, Qinghai Provincial People's Hospital, Xining, Qinghai 810006, P.R. China; [5]Department of Neurosurgery, High-Altitude Disease Clinical Medical Research Center of Qinghai Province, Qinghai Provincial People's Hospital, Xining, Qinghai 810006, P.R. China

Received June 9, 2026; Accepted September 18, 2026

DOI: 10.3892/mmr.2026.14042

Abstract. High-altitude cerebral edema (HACE) is a life-threatening complication of acute high-altitude exposure, but effective treatment strategies remain limited. The influence of Piezo1 on the tight junctions of brain microvascular endothelial cells in HACE was examined to identify novel therapeutic interventions against HACE. A mouse model of HACE was established through exposure to a simulated high-altitude hypobaric hypoxia environment. Brain water content, Evans Blue staining, magnetic resonance imaging, hematoxylin and eosin staining, FITC-Dextran leakage assay and transmission electron microscopy were utilized to evaluate the impact of Piezo1 on HACE. A cell model of HACE was created by subjecting bEnd.3 cells to high fluid shear stress (HFSS) and hypoxic conditions. The effects of Piezo1 and Calpain-1 on tight junction protein expression were assessed via western blot analysis. Mice with HACE exhibited increased brain water content, disrupted blood-brain barrier integrity, enhanced microvascular permeability, hippocampal and cortical damage and reduced expression of VE-cadherin, occludin, claudin-5 and ZO-1 proteins, alongside elevated Piezo1 and Calpain-1 activity in brain microvascular endothelial cells. Silencing of Piezo1 alleviated these HACE symptoms. bEnd.3 cells subjected to HFSS and hypoxia showed increased intracellular Ca^{2+}, along with heightened Calpain-1 protein expression and activity, while levels of VE-cadherin, occludin, claudin-5 and ZO-1 proteins were diminished. Both Piezo1 silencing and Calpain-1 inhibition reversed these *in vitro* changes. Notably, Piezo1 silencing reduced Calpain-1 activity without significantly altering Calpain-1 protein levels. Piezo1 silencing may ameliorate HACE by enhancing tight junctions in brain microvascular endothelial cells through the suppression of calcium influx-mediated Calpain-1 activity. Thus, targeting Piezo1 expression may represent a promising therapeutic approach for HACE.

Correspondence to: Dr Qiang Zhang, Department of Neurosurgery, High-Altitude Disease Clinical Medical Research Center of Qinghai Province, Qinghai Provincial People's Hospital, 2 Gonghe Road, Xining, Qinghai 810006, P.R. China
E-mail: jakiyocao@mailbox.qhu.edu.cn

Key words: high-altitude cerebral edema, brain water content, Piezo1, calpain-1 activity, tight junction

Introduction

High-altitude cerebral edema (HACE) is a life-threatening encephalopathy resulting from exposure to high-altitude hypoxic conditions, where disruption of the blood-brain barrier (BBB) serves as the primary pathological factor, with altered mental status and ataxia as the main clinical manifestations (1). Numerous animal studies indicate that high-altitude hypoxia impairs tight junctions in brain microvascular endothelial cells, which notably contributes to BBB disruption and subsequent cerebral edema (2,3). Recent investigation demonstrated that restoring tight junction integrity and reducing the permeability of brain microvascular endothelial cells represent promising strategies to mitigate BBB disruption in HACE treatment (4). These findings highlight the importance of a comprehensive understanding of the mechanisms driving tight junction disruption in brain microvascular endothelial cells under high-altitude hypoxic conditions.

HACE induces abnormal microvascular blood flow in the brain, leading to abrupt changes in fluid shear stress (FSS) experienced by brain microvascular endothelial cells. FSS is a primary mechanical force exerted by blood flow on these cells. High FSS (HFSS) reduces tight junction protein expression, compromising barrier function and elevating endothelial permeability, a key mechanism behind BBB disruption (5). Under hypoxic conditions, endothelial metabolic dysfunction

and oxidative stress markedly impair cell viability and barrier function (6). Piezo1, a mechanosensitive cation channel, possesses a unique mechanosensitive structure that enables the detection of changes in cell membrane tension, converting mechanical forces, such as shear stress and tensile stress, into electrical signals or Ca^{2+} influx to regulate blood flow (6). Up-regulation of Piezo1 has been observed in rats with hypoxic-ischemic brain injury, while its inhibition reduces brain damage in such models (7). In rats with vascular dementia induced by chronic cerebral hypoperfusion, suppression of Piezo1 enhances BBB integrity and maintains brain microvascular structure (8). Furthermore, in mice subjected to cerebral ischemia/reperfusion injury, Piezo1 expression markedly increases in cerebral vascular endothelial cells, while Piezo1 knockdown alleviates BBB disruption by preventing the degradation of proteins critical to BBB integrity (9). Collectively, these findings suggest that Piezo1 knockdown protects BBB integrity in brain injuries caused by hypoxia and ischemia; however, its role in HACE has yet to be reported. The present study represents the initial investigation of the impact of Piezo1 on HACE, particularly concerning tight junctions in brain microvascular endothelial cells.

Calpain-1, a calcium-dependent protease functioning as a downstream effector of Piezo1, is activated upon elevated intracellular Ca^{2+} levels and modulates cellular functions through the specific cleavage of target proteins, including vascular endothelial cadherin (VE-cadherin) and occludin (10,11). Excessive activation of Calpain-1 is linked to increased BBB permeability and cerebral edema following hyperlipidemia-induced focal cerebral ischemia (12). In mice with traumatic brain injury, Calpain-1 inhibition preserves BBB integrity by enhancing tight junction function in brain microvascular endothelial cells (13). Based on this evidence, the current study investigated, for the first time, whether Piezo1 contributes to HACE regulation by modulating calcium influx-mediated Calpain-1 activity.

Materials and methods

Establishment of a mouse model of HACE. C57BL/6 mice (male, 8 weeks old, 20-22 g; n=168) were obtained from Changzhou Cavens Laboratory Animal Co., Ltd. Piezo1 conditional knockout (CKO) mice (male, 8 weeks old, 20-22 g; n=48) were generated by Cyagen Biosciences, Inc. Cas9 protein, two guide RNAs (gRNA-1: 5'-GGACTGCCAGAC ACTGTTTAGGG-3' and gRNA-2: 5'-CTGCTCTCTTGT CTCATGCGTGG-3'), and a donor vector containing two loxP sequences flanking Exons 3-5 of the mouse Piezo1 gene were co-injected into fertilized eggs. The gRNA-to-target sequence alignments were shown in Fig. S1A and B. The embryos were then transferred to recipient female mice to obtain F0 founder mice. Genotyping of F0 founders and subsequent generations was performed by PCR amplification using two pairs of allele-specific primers: Pair 1 (F1: 5'-AGCAAGGCC AATGTAGTATCTGG-3', R1: 5'-CTATTGGTGCCTAGT TGGCAGAC-3') spanning the 5' loxP insertion site, and Pair 2 (F2: 5'-CGGCTCCCAGTGACAGTTTTGAT-3', R2: 5'-GTG GATTCGGACCAGTCTGA-3') spanning the 3' loxP insertion site. These primer pairs were designed specifically against the floxed allele and will not amplify the wild-type Piezo1 locus. Positive PCR products were further confirmed by Sanger sequencing to verify correct loxP insertion. F0 founder mice carrying the correctly targeted allele were backcrossed with wild-type C57BL/6J mice to generate heterozygous F1 offspring ($Piezo1^{flox/+}$). Subsequent intercrossing yielded homozygous $Piezo1^{flox/flox}$ mice for experimental use.

Mice were housed in a constant temperature environment at 25˚C under a 12-h light-dark cycle. Standard feed and water were provided *ad libitum*. Prior to experimentation, a 7-day acclimation period was allowed. The Animal Ethics Committee of Qinghai Provincial People's Hospital approved all animal experiments [approval no. (2023)-246]. The mouse model of HACE was established as follows: Mice were placed in a hypobaric chamber and subjected to simulated altitude conditions of 7,600 m (25,000 ft, 282 mmHg) at a descent velocity of 300 m/min for 12, 24, 48 and 72 h, respectively. After exposure, mice were returned to sea level at a descent velocity of 300 m/min. Following the experiment, mice were anesthetized via inhalation of 5% isoflurane and maintained under anesthesia with 1.5% isoflurane. Deep anesthesia was confirmed once the mice were unresponsive to stimulation of the head, tail, limbs or body. Then they were perfused with physiological saline (0.9%) to clear blood. After perfusion, mice were already dead (the fluid flowing from the incision in the right atrium became clear and free of blood; mice became completely rigid). Then the whole brains were quickly collected and stored in a cryogenic freezer at -80˚C. Mice maintained under normal conditions served as controls, with each group comprising 24 mice. Animal grouping and detailed tests were as follows:

Part I. A total of 120 C57BL/6 mice were randomly selected and divided into the Control group, the H-12, H-24, H-48 and H-72 h groups, with 24 mice per group. Within each group of 24, six mice were designated for brain water content measurement, six for Evans blue (EB) staining, six for the Fluorescein isothiocyanate (FITC)-Dextran leakage assay and the remaining six for hematoxylin and eosin (H&E) staining, immunofluorescence staining, transmission electron microscopy, proteomics analysis, western blot analysis and reverse transcription-quantitative polymerase chain reaction (RT-qPCR).

Part II. The remaining 48 C57BL/6 mice and the 48 Piezo1 knockdown mice were utilized. The 48 C57BL/6 mice were randomly divided into the Control and H-24 h groups, with 24 mice per group. The 48 Piezo1 knockdown mice were randomly assigned to the CKO-Piezo1 and CKO-Piezo1 + H-24 groups, with 24 mice per group. For each group of 24 mice, six were used for brain water content measurement, six for EB staining, six for FITC-Dextran leakage assay and the remaining six for H&E staining, western blot analysis and Calpain-1 activity detection.

In the animal experiments, randomization and blinding were employed. After the 1-week acclimatization period, a researcher not involved in subsequent experimental procedures or data analysis randomly assigned animals to groups using a random number table generated by Excel (Microsoft Corporation). Blinding involved different researchers conducting experimental procedures and evaluating results. All samples were labeled with numerical

codes, and results were unblinded only after statistical analysis was completed.

Measurement of brain weight/body weight ratio. Before euthanasia, the weight of each mouse was recorded, followed by measurement of whole brain weight. The extent of cerebral edema was quantified as the percentage of brain weight relative to body weight.

Detection of brain water content. Subsequently, the whole brains of the mice were placed in an 80˚C drying oven for 72 h to determine dry weight. Brain water content was calculated using the formula (wet weight-dry weight)/wet weight x100%.

BBB permeability detection. BBB permeability was assessed via tail vein injection of EB dye. Following HACE modeling, mice received a tail vein injection of a 2% EB saline solution (4 ml/kg) (Nanjing Senbeiga Biotechnology Co., Ltd.) and were allowed to circulate for 1 h. Under anesthesia, mice were perfused with physiological saline (0.9%) to clear the intravascular dye. After euthanasia, the brains were collected and homogenized in a 50% trichloroacetic acid solution. The resulting mixture was centrifuged (15,000 x g, 30 min), and the supernatant was diluted 1:3 in ethanol. The absorbance of the diluted supernatant was measured using a microplate reader (Thermo Fisher Scientific, Inc.) at a wavelength of 630 nm to determine EB content, calculated using the formula (EB concentration derived from the standard curve x dilution factor)/brain tissue weight.

Magnetic resonance imaging (MRI) examination and evaluation of apparent diffusion coefficient (ADC). After anesthesia with 1.5% isoflurane, mice underwent MRI examination using a 7.0 T BioClinScan animal system (Bruker Corporation). Multislice coronal spin-echo diffuse-weighted images were acquired using an echo planar diffusion-trace MRI sequence (matrix size=64x64, TE=23.82 msec, TR=2,500 msec, slice thickness=1.0 mm, b value=1,030.5 sec/mm^2). Diffuse-weighted images were reconstructed using Para Vision version 5.1 software (Bruker Corporation). Water diffusion was evaluated by calculating the ADC values using the formula-ln(S/S0)/b, where S and S0 represent signals acquired with and without diffusion weighting, respectively.

H&E staining. Brains were fixed in 4% paraformaldehyde for 24 h at 4˚C and embedded in paraffin, subsequently sectioned to a thickness of 4 μm. Sections were baked for 1 h at 60˚C in a drying oven. After conventional dewaxing and rehydration, staining was performed using H&E solutions (Shanghai Lianmai Biological Engineering Co., Ltd.). Hematoxylin solution was utilized to stain the sections for 5 min at room temperature, while eosin staining was performed for 1 min at room temperature. Following dehydration and transparency, sections were mounted in neutral resin and examined for pathological changes in the hippocampus and cerebral cortex using an optical microscope (Olympus Corporation).

FITC-Dextran leakage assay. Cerebral microvascular permeability was evaluated using a FITC-Dextran leakage assay. Mice received an intraperitoneal injection of 70 kDa FITC-dextran (Shanghai Maokang Biotechnology Co., Ltd.) at a dosage of 125 μg/g. After 2 h, mice were anesthetized with 1.5% isoflurane and perfused with physiological saline (0.9%). After euthanasia, the brains were harvested and fixed for 24 h at 4˚C in 4% paraformaldehyde, then sectioned to a thickness of 4 μm. Sections were probed overnight at 4˚C with mouse anti-CD31 primary antibody (1:100; HY-P80599; MedChemExpress) and subsequently reacted with Alexa Fluor 555-labeled goat anti-mouse secondary antibody (1:200; HY-P81006; MedChemExpress) for 2 h at room temperature. Following 4',6-diamidino-2-phenylindole (DAPI) (Nanjing Jiancheng Bioengineering Institute) staining of cell nuclei for 5 min at room temperature, brain sections were observed under a confocal microscope (Olympus Corporation). The fluorescence intensity of FITC-Dextran was quantified using ImageJ software (Version 1.54r; National Institutes of Health).

Transmission electron microscope (TEM). Following fixation in 4% paraformaldehyde (for 24 h at 4˚C), mouse brains were embedded in epoxy resin (at 60˚C for 48 h), and then dehydrated and sectioned into 60-nm ultrathin sections. The sections were stained with 4% uranyl acetate (for 30 min at room temperature) and then 0.3% lead citrate (for 8 min at room temperature), enabling examination of tight junctions in cerebral microvessels using a TEM (HT7700; Hitachi, Ltd.).

Isolation of mice brain microvascular endothelial cells. Brain microvascular endothelial cells were isolated from mice as previously described (14). Fresh mouse brains were collected and placed in a culture dish containing D-Hanks' medium (Shanghai Yuanye Bio-Technology Co., Ltd.). Under a stereomicroscope (Leica Microsystems GmbH), white matter, pia mater and large blood vessels were carefully removed. The remaining cerebral cortex was rinsed with D-Hanks' solution and sectioned into 1 mm^3 pieces, which were incubated with 0.1% type II collagenase (Beijing BioLab Technology Co., Ltd.) for 40 min in a 37˚C water bath. The mixture was then centrifuged at 250 x g for 3 min, allowing collection of microvascular endothelial cells from the pellet for downstream analyses, including RT-qPCR, western blot analysis and Calpain-1 activity detection.

Proteomics analysis and Kyoto Encyclopedia of Genes and Genomes (KEGG) enrichment analysis. Brain tissues from mice were lysed in radio-immunoprecipitation assay (RIPA) lysis buffer (Jiangsu KeyGEN BioTECH Co., Ltd.) to extract total proteins. Total protein concentration was determined using a Bicinchoninic Acid Assay (BCA) kit (Jiangsu KeyGEN BioTECH Co., Ltd.). Protein samples were loaded onto a trap column (flow rate, 350 nl/min) and an analytical column, followed by proteomic analysis using a Tims Time-of-Flight (TOF) Pro mass spectrometer (Thermo Fisher Scientific, Inc.) equipped with an EasySpray source (Thermo Fisher Scientific, Inc.). Data were analyzed with Spectronaut Pulsar 18.4 (Biognosys AG), with the uniprot-Mus musculus-10090-2024.2.1.fasta as the search database (https://www.uniprot.org/). Differentially expressed proteins were identified based on the criteria of fold change ≥2 or ≤0.5 and P<0.05. A heatmap of the

differentially expressed proteins was generated using R software (version 4.3.1; R Foundation for Statistical Computing), with expression levels of Piezo1, VE-cadherin and occludin presented in statistical graphs. KEGG enrichment analysis was performed using the Database for Annotation, Visualization, and Integrated Discovery (DAVID) functional annotation tool (https://davidbioinformatics.nih.gov/).

Cell culture, transfection and treatment. Mouse brain microvascular endothelial cells (bEnd.3 cells) obtained from Shanghai Kelei Biopharmaceutical Technology Co., Ltd., were cultured in standard medium consisting of 89% Dulbecco's modified Eagle medium (DMEM), 10% fetal bovine serum (FBS) and 1% penicillin-streptomycin at 37˚C under normoxic conditions (5% CO_2 and 95% air). DMEM, FBS and penicillin-streptomycin were sourced from Beyotime Biotechnology. For hypoxia treatment, bEnd.3 cells were maintained in standard medium at 37˚C under hypoxic conditions (5% CO_2, 94% N_2 and 1% O_2).

Piezo1 small interfering RNA (siRNA; sense: GCC CUGGUACUCAACACUATT; antisense: UAGUGUUGA GUACCAGGGCTT), siRNA negative control (NC) (sense: UUCUCCGAACGUGUCACGUTT; antisense: ACGUGA CACGUUCGGAGAATT), NC vectors and Piezo1 overexpression vectors were procured from Shanghai GeneChem Co., Ltd. bEnd.3 cells, seeded in serum-free medium, were transfected with siRNA (50 nM) or vectors (2 μg) using Lipofectamine 3000 (Thermo Fisher Scientific, Inc.) for 8 h at 37˚C. Post-transfection, cells were cultured for 48 h in standard medium at 37˚C under normoxic conditions (5% CO_2 and 95% air), and then collected for subsequent experiments.

Reports indicate that high-altitude sickness can lead to a marked increase in blood FSS, thereby causing vascular endothelial dysfunction, the core pathological mechanism behind BBB disruption. To simulate this key hemodynamic change, bEnd.3 cells were subjected to HFSS (5,15,16). According to previously reported protocols (17,18), HFSS simulation was performed as follows: bEnd.3 cells plated on flow chamber slides (Ibidi GmbH) were exposed to shear stress levels of 10, 20, 30, or 40 dyn/cm^2 for 24 h at 37˚C. The culture medium was circulated over the cell monolayer using an IBIDI pump system (Ibidi GmbH), with a shear stress of 10 dyn/cm^2 serving as the control condition.

Calpain-1 activity was inhibited using PD150606 (MedChemExpress) at a concentration of 50 μM for 24 h at 37˚C. Yoda1 (MedChemExpress), a specific Piezo1 agonist, was applied at 5 μM to treat cells for 24 h at 37˚C. Additionally, PD151746 (MedChemExpress) was used to inhibit Calpain-1 at a concentration of 10 μM by treating cells for 24 h at 37˚C. Calcium chelator 1,2-bis-(2-aminophenoxy) ethane-N,N,N',N'-tetraacetic acid acetoxymethyl ester (BAPTA-AM) (MedChemExpress) was utilized to treat cells for 24 at 10 μM. The mechanism of action of BAPTA-AM is to rapidly bind free Ca^{2+} within the cell with high affinity, thereby buffering calcium signaling.

Cell grouping. Cell grouping and specific processing were structured as follows.

Experiment I. Experiment I comprised the control group, si-NC group and si-Piezo1 group. bEnd.3 cells in the control group were cultured in normal medium and maintained under normoxic conditions (5% CO_2 and 95% air) for 24 h. Cells in the si-NC and si-Piezo1 groups were separately transfected with siRNA NC and Piezo1 siRNA, respectively, followed by culturing in normal medium under normoxic conditions for 24 h.

Experiment II. Experiment II included the si-NC group, HFSS + si-NC group, and HFSS + si-Piezo1 group. Cells from all three groups were maintained under two distinct conditions for 24 h: Normoxia (5% CO_2 and 95% air) and hypoxia (5% CO_2, 94% N_2 and 1% O_2). Under these conditions, bEnd.3 cells in the si-NC group were transfected with siRNA NC and exposed to a shear stress of 10 dyn/cm^2. Cells in the HFSS + si-NC and HFSS + si-Piezo1 groups were transfected with siRNA NC and Piezo1 siRNA, respectively, and subjected to a shear stress of 30 dyn/cm^2.

Experiment III. Experiment III included the control group, HFSS group, and HFSS + PD150606 group. Under both normoxic (5% CO_2 and 95% air) and hypoxic conditions (5% CO_2, 94% N_2, and 1% O_2), bEnd.3 cells in the control group received no additional treatment. In the HFSS group and HFSS + PD150606 group, cells were treated without or with 50 μM PD150606, respectively, in the presence of 30 dyn/cm^2 shear stress. All groups were maintained under their respective conditions for 24 h.

Experiment IV. Experiment IV comprised the control group, model group, Yoda1 group, and Model + Yoda1 group. Cells in the control group were maintained under normoxic conditions (5% CO_2 and 95% air) for 24 h. The Model group was exposed to hypoxia (5% CO_2, 94% N_2, and 1% O_2) for 24 h at 37˚C. The Yoda1 group was treated with 5 μM Yoda1 for 24 h under normoxic conditions, while cells in the Model + Yoda1 group were cultured in hypoxic conditions for 24 h at 37˚C in the presence of 5 μM Yoda1.

Experiment V. Experiment V included the Vector group, Piezo1-OE group, Vector + PD151746 group, and Piezo1-OE + PD151746 group. Cells in the Vector and Piezo1-OE groups were separately transfected with NC vectors and Piezo1 overexpression vectors and subsequently cultured under normoxic conditions (5% CO_2 and 95% air) for 24 h. The Vector + PD151746 group was transfected with NC vectors and then exposed to 10 μM PD151746 for 24 h under normoxic conditions. Cells in the Piezo1 + PD151746 group were transfected with Piezo1 overexpression vectors and subsequently treated with 10 μM PD151746 for 24 h under normoxic conditions.

Experiment VI. Experiment VI included the Vector group, Vector + BAPTA-AM group, Piezo1-OE group, and Piezo1 + BAPTA-AM group. Cells in the Vector and Piezo1-OE groups were separately transfected with NC vectors and Piezo1 overexpression vectors. Those in the Vector + BAPTA-AM group were transfected with NC vectors and then exposed to BAPTA-AM at 10 μM for 24 h. Cells in the Piezo1 + BAPTA-AM group were transfected with Piezo1 overexpression vectors and subsequently treated with 10 μM BAPTA-AM for 24 h.

RT-qPCR. Total RNA was extracted from bEnd.3 cells and mouse brain microvascular endothelial cells using TRIzol

reagent (Shanghai Yuanye Bio-Technology Co., Ltd.), followed by complementary DNA synthesis employing a PrimeScript™ RT reagent Kit (Shanghai Shanran Biotechnology Co., Ltd.). Quantitative RT-qPCR was conducted using SYBR Green Master Mix (Thermo Fisher Scientific, Inc.) on an ABI 7500 Real-Time PCR System (Applied Biosystems; Thermo Fisher Scientific, Inc.). The amplification program included an initial denaturation at 95˚C for 3 min, followed by 40 cycles of 10 sec at 95˚C and 30 sec at 60˚C. The primer sequences were as follows: *Piezo1*, forward: CCTGTTACGCTTCAATGCTCT, reverse: GTGTAGGCATATCTGAAAGGCAA; *Calpain-1*, forward: GGGGAGTTCTGGATGTCGTT, reverse: GGT GCCCTCGTAAAATGTGGT; *β-actin*, forward: GGCTGT ATTCCCCTCCATCG, reverse: CCAGTTGGTAACAAT GCCATGT (all synthesized by Shanghai GeneChem Co., Ltd.). Relative *Piezo1* mRNA expression was quantified using the $2^{-\Delta\Delta Cq}$ method (19), with *β-actin* serving as the endogenous control. Alignment of genotyping primers to the floxed Piezo1 allele and β-actin were shown in Fig. S1C.

Western blot analysis. Total proteins from bEnd.3 cells and mouse brain microvascular endothelial cells were extracted using RIPA lysis buffer (Jiangsu KeyGen Biotech Co., Ltd.). Isolation of mouse brain microvascular endothelial cells was conducted as previously described (20). Total protein concentration was quantified using a BCA kit (Jiangsu KeyGen Biotech Co., Ltd.). Proteins (30 μg per lane) were separated on 10% gels using sodium dodecyl sulfate-polyacrylamide gel electrophoresis and subsequently transferred to polyvinylidene fluoride (PVDF) membranes. Membranes were blocked with 5% skimmed milk (Shanghai Xinfan Biological Technology Co., Ltd.) for 1 h at room temperature. Primary antibodies were applied for 12 h at 4˚C, including rabbit anti-Piezo1 (1:1,000; 28511-1-AP; Proteintech Group, Inc.), rabbit anti-Calpain-1 (1:500; 23048R; Hangzhou Lianke Meixun Biomedical Technology Co., Ltd.), rabbit anti-VE-cadherin (1:1,000, HY-P86361; MedChemExpress), rabbit anti-occludin (1:1,000; CY-10011R; Hangzhou Lianke Meixun Biomedical Technology Co., Ltd.), rabbit anti-claudin-5 (1:1,000; ABP50990; AmyJet Scientific, Inc.), rabbit anti-zonula occludens-1 (ZO-1; 1:500; K27853-UOR; Beijing BioLab Technology Co., Ltd.), mouse anti-Spectrin (1:1,000; sc-53444; Santa Cruz Biotechnology, Inc.), rabbit anti-spectrin breakdown products (SBDP, also termed SNTF; 1:10,000; cleaved all-spectrin; ABN2264; MilliporeSigma) and rabbit anti-β-actin (1:2,000; HY-P87821; MedChemExpress). Membranes were subsequently incubated with horseradish peroxidase-conjugated goat anti-rabbit (1:10,000; 111-035-003; AmyJet Scientific, Inc.) or goat anti-mouse secondary antibodies (1:10,000; 1030-05; AmyJet Scientific, Inc.) for 2 h at room temperature. Protein bands were visualized using enhanced chemiluminescent reagent (Shanghai Yuanmu Biotechnology Co., Ltd.) and semi-quantified with ImageJ software (Version 1.54r; National Institutes of Health), with β-actin as the internal reference.

Immunofluorescence staining. Following fixation with 4% paraformaldehyde for 24 h at 4˚C, mouse brain sections (4 μm) and bEnd.3 cells subjected to various treatments were permeabilized with 0.5% Triton X-100 (Shanghai Xitang Biotechnology Co., Ltd.) for 20 min at room temperature and blocked with normal goat serum (Wuhan Chundu Biotechnology Co., Ltd.) for 1 h at room temperature. For detection of Piezo1 in mouse brain microvascular endothelial cells, sections were incubated overnight at 4˚C with rabbit anti-Piezo1 primary antibody (1:100; 28511-1-AP; Proteintech Group, Inc.) and mouse anti-CD31 primary antibody (1:100; HY-P80599; MedChemExpress), followed by incubation with Alexa Fluor 555-conjugated goat anti-rabbit secondary antibody (1:200; GD-X0295G-AF555; Shanghai Guduo Biotechnology Co., Ltd.) and Alexa Fluor 488-conjugated goat anti-mouse secondary antibody (1:200, YT859-RJG, BioLab Technology, Beijing, China) for 2 h at room temperature. To visualize Piezo1 and Calpain-1 in bEnd.3 cells, rabbit anti-Piezo1 primary antibody (1:100; 28511-1-AP; Proteintech Group, Inc.) and rabbit anti-Calpain-1 primary antibody (1:100; 23048R; Hangzhou Lianke Meixun Biomedical Technology Co., Ltd.) were employed (overnight at 4˚C), followed by Alexa Fluor 488-conjugated goat anti-rabbit secondary antibody (1:200; yb0423; Shanghai Yubo Biotechnology Co., Ltd.) (for 2 h at room temperature). After nuclear staining with DAPI for 5 min at room temperature, sections and cells were dried, mounted in neutral resin and observed under a confocal microscope (Olympus Corporation). Protein expression was quantified using ImageJ software.

Fluo4-AM fluorescent probe detection. Intracellular Ca^{2+} levels in bEnd.3 cells were assessed using the Fluo4-AM fluorescent probe. Cells from each experimental group were incubated with Fluo4-AM (Beijing BioLab Technology Co., Ltd.) for 30 min at room temperature. Fluorescence intensity was monitored with a fluorescence microscope (Olympus Corporation) and quantified using ImageJ software.

Calpain-1 activity detection. Calpain-1 activity was measured with a commercial assay kit (cat. no. KA0723; AmyJet Scientific, inc.). Cells and mouse brain microvascular endothelial cells were collected and suspended in a buffer containing 100 mM Tris-HCl, 1 mM dithiothreitol, 0.5 mM phenylmethylsulfonyl fluoride, 5 mM ethylenediaminetetraacetic acid, 5 mM benzamidine and 10 mM β-mercaptoethanol. The mixture was ultrasonicated four times (10 sec each) at 4˚C with 1-min intervals, followed by centrifugation at 15,000 x g for 20 min. Calpain-1 activity was assessed with 40 μg of supernatant, 15 mM calcium (in 50 μl buffer) and 100 μM fluorogenic calpain substrate (AmyJet Scientific, Inc.), with excitation at 320 nm and emission at 480 nm. Calpain-1 activity was quantified using ImageJ software.

Cell counting kit-8 (CCK-8) assay. Cell viability of bEnd.3 cells was evaluated using a CCK-8 assay. Cells were seeded in 96-well plates and incubated with 10 μl CCK-8 solution (Jiangsu KeyGen Biotech Co., Ltd.) for 2 h at 37˚C. Optical density (OD) values were measured on a microplate reader (Huisong Pharmaceuticals) to estimate cell viability. Cell viability was quantified using the formula: [(OD value of the experimental group-OD value of the blank group)/(OD value of the control group-OD value of the blank group)] x100.

Trans-endothelial electrical resistance (TEER) measurement. TEER of bEnd.3 cells was measured using an epithelial

voltmeter (Beijing Donggong Technology Co., Ltd.). Cells were seeded on inserts at a density of $5x10^4$ cells per insert and subjected to the respective treatment conditions. Following the removal of the culture medium, inserts were transferred to new wells and washed with phosphate-buffered saline. Resistance across the cells was recorded and analyzed. TEER was quantified using the formula: (Resistance value measured in the chamber containing a monolayer of cells-the background resistance value measured in the blank chamber without cells) x the area of the polycarbonate membrane at the bottom of the inserts.

Statistical analysis. Data analysis was performed using a blinded method. One researcher performed animal grouping and data collection, while another independent researcher evaluated the results without knowledge of group assignments. All samples were labeled with numerical codes, with the blinded status revealed only after the analysis of all data was completed.

Data are expressed as mean ± standard deviation. Statistical analysis was conducted using GraphPad Prism 8.0 software (Dotmatics). Error bars represented standard deviation, reflecting the dispersion of individual observations around the group mean. Normality of data distribution was assessed using the Shapiro-Wilk test. Intergroup statistical differences were compared via Student's t-test (for two distinct groups) or one-way analysis of variance (ANOVA) with post-hoc Tukey's test (for more than two distinct groups). $P<0.05$ was considered to indicate a statistically significant difference.

Results

Hypobaric hypoxia exposure resulted in cerebral edema and increased BBB permeability in mice. To establish a mouse model of HACE, C57BL/6 mice were exposed to a hypobaric hypoxia environment for varying durations. Cerebral edema was assessed by measuring the ratio of brain weight to body weight (Fig. 1A) and brain water content (Fig. 1B). Mice subjected to hypobaric hypoxia for 24, 48 and 72 h exhibited significantly increased brain weight/body weight ratios and brain water content, with the most pronounced elevation observed in the 24-h exposure group (H-24, H-48 and H-72 h vs. control group; $P<0.001$ for the ratio of brain weight to body weight at H-24, H-48 and H-72 h; $P<0.001$ for the brain water content at H-24 h; $P<0.01$ for the brain water content at H-48 h; $P<0.05$ for the brain water content at H-72 h). Additionally, enhanced BBB permeability, indicated by significantly higher EB content, was observed in mice treated with hypobaric hypoxia for 24, 48 and 72 h, especially in the 24-h group (H-24, H-48 and H-72 h vs. control group; $P<0.001$; Fig. 1C). Alterations in ADC values on brain MRI reflect changes in brain tissue water content, thus facilitating assessment of brain water content (21). The MRI images are shown in Fig. 1D. Significantly reduced ADC values were recorded in mice exposed to hypobaric hypoxia for 12, 24 and 48 h (H-12, H-24 and H-48 h vs. control group; $P<0.05$ at H-48 h, $P<0.001$ at H-12 h and at H-24 h; Fig. 1E). H&E staining revealed notable cellular edema (black arrows) and nuclear condensation (red arrows) in the hippocampus and cerebral cortex of mice, particularly in those exposed for 24 h (Fig. 1F). Thus, hypobaric hypoxia exposure resulted in marked cerebral edema and increased BBB permeability in mice, with 24-h exposure eliciting the most significant effects, leading to its selection for subsequent studies.

Hypobaric hypoxia exposure caused elevated microvascular permeability, impaired tight junctions and increased Piezo1 expression in mice. TEM images revealed impaired tight junctions in brain microvessels of mice exposed to hypobaric hypoxia for 24 h (H-24 h vs. control group; Fig. 2A). A FITC-Dextran leakage assay was conducted to assess brain microvascular permeability, complemented by CD31 immunofluorescence staining to localize brain microvascular endothelial cells. Increased microvascular permeability was observed in the brains of mice after 24 h of hypobaric hypoxia exposure (H-24 h vs. control group; $P<0.001$; Fig. 2B). A heatmap of differentially expressed proteins generated through proteomics analysis showed differences between control mice and those exposed to hypobaric hypoxia for 24 h (Fig. 2C). KEGG enrichment analysis indicated an association between these differentially expressed proteins and tight junctions, specifically the pathway 'Cell adhesion molecules' was identified, with its associated proteins significantly downregulated (Fig. 2D). Proteomics analysis demonstrated up-regulation of Piezo1 and down-regulation of VE-cadherin and occludin within the brain microvascular endothelial cells of mice subjected to hypobaric hypoxia for 24 h (H-24 h vs. control group; $P<0.001$; Fig. 2E).

To investigate Piezo1 expression in brain microvascular endothelial cells, these cells were isolated and subjected to RT-qPCR and western blot analyses. Increased mRNA ($P<0.01$) and protein levels ($P<0.001$) of Piezo1 were observed in brain microvascular endothelial cells of mice after 24 h of hypobaric hypoxia exposure (H-24 h vs. control group; Fig. 2F and G). Immunofluorescence staining of CD31/Piezo1 was performed to visualize Piezo1 expression within brain microvascular endothelial cells, revealing enhanced expression after 24 h of hypobaric hypoxia exposure (H-24 h vs. control group; $P<0.001$; Fig. 2H). These results indicate that a hypobaric hypoxia environment leads to increased microvascular permeability, impaired tight junctions and enhanced Piezo1 expression in brain microvascular endothelial cells.

Piezo1 silencing caused a decline in intracellular Ca^{2+} levels and Calpain-1 activity within the HFSS- and hypoxia-induced bEnd.3 cells. bEnd.3 cells were subjected to FSS at 10, 20, 30 and 40 dyn/cm^2 for 24 h. A significant increase in Piezo1 protein expression was observed as FSS levels rose ($P<0.01$, $P<0.001$). Notably, Piezo1 protein levels in cells exposed to 40 dyn/cm^2 were comparable to those in cells exposed to 30 dyn/cm^2. Consequently, HFSS at 30 dyn/cm^2 was designated as HFSS for subsequent experiments (Fig. S2A). Transfection of Piezo1 siRNA into bEnd.3 cells resulted in a significant reduction in Piezo1 protein expression compared with the siRNA NC (si-Piezo1 vs. si-NC; $P<0.001$; Fig. S2B).

Under both normoxic and hypoxic conditions, HFSS treatment significantly elevated Piezo1 mRNA and protein expression in bEnd.3 cells (HFSS + si-NC vs. si-NC; $P<0.001$). Transfection with Piezo1 siRNA led to decreased expression of Piezo1 mRNA and protein in HFSS-treated cells under both

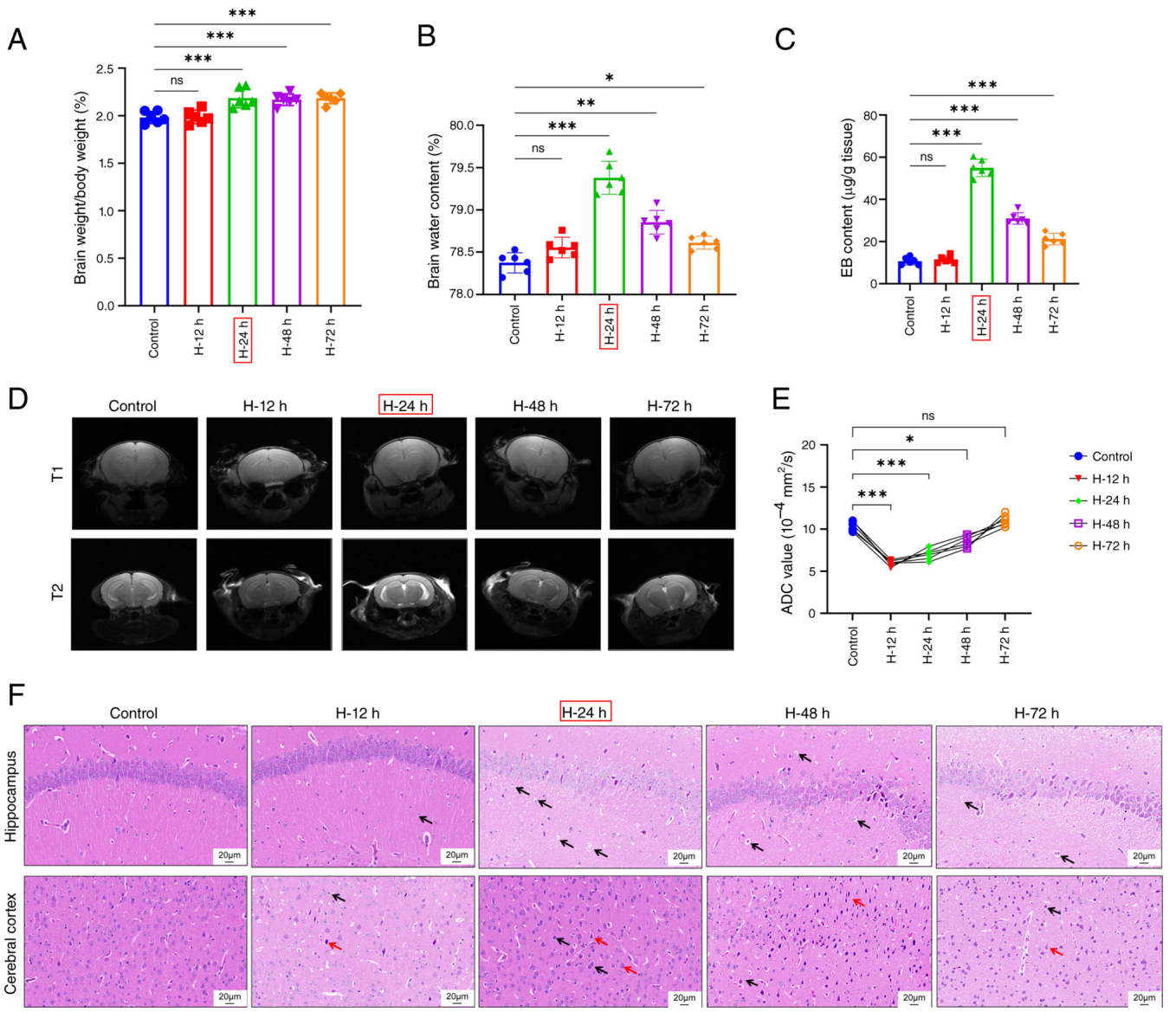


Figure 1. Hypobaric hypoxia exposure led to cerebral edema in mice. (A) Mice exposed to a hypobaric hypoxia environment for 24, 48 and 72 h showed higher brain weight/body weight ratios (n=6). (B) Exposure to a hypobaric hypoxia environment for 24, 48 and 72 h caused a significant elevation in brain water content (n=6). (C) EB staining showed exacerbated blood-brain barrier permeability in mice following 24, 48 and 72 h of hypobaric hypoxia exposure (n=6). (D) MRI images of mouse brains and (E) statistical analysis of ADC values (n=6). (F) H&E staining showed that mice exposed to hypobaric hypoxia conditions exhibited cellular edema (indicated by black arrows) and nuclear condensation (indicated by red arrows) in the hippocampus and cerebral cortex (n=6). *P<0.05, **P<0.01 and ***P<0.001 vs. control group. Statistical tests were performed using ANOVA with post-hoc Tukey's test. Error bars represent SD, reflecting the dispersion of individual observations around the group mean. H, hypoxia; EB, Evans Blue; ADC, apparent diffusion coefficient.

conditions (HFSS + si-Piezo1 vs. HFSS + si-NC; P<0.001; Fig. 3A and B). Western blot analysis revealed that HFSS treatment increased Calpain-1 protein expression in bEnd.3 cells under normoxia and hypoxia (HFSS + si-NC vs. si-NC; P<0.001). Notably, Piezo1 silencing did not significantly affect Calpain-1 protein expression in HFSS-treated cells under either condition (HFSS + si-Piezo1 vs. HFSS + si-NC; Fig. 3A and C). Immunofluorescence staining (Fig. 3D and E) and detection with the Fluo4-AM fluorescent probe (Fig. 3F) were employed to monitor the expression of Piezo1 and Calpain-1 proteins, as well as intracellular Ca^{2+} levels in bEnd.3 cells. Following exposure to normoxic and hypoxic conditions, HFSS-treated bEnd.3 cells exhibited elevated levels of Piezo1 and Calpain-1 proteins, along with increased intracellular Ca^{2+} levels (HFSS + si-NC vs. si-NC; P<0.001). By contrast, cells subjected to both Piezo1 siRNA transfection and HFSS treatment demonstrated reduced Piezo1 protein expression and intracellular Ca^{2+} levels (HFSS + si-Piezo1 vs. HFSS + si-NC; P<0.001). However, under HFSS conditions, Piezo1 silencing did not significantly affect Calpain-1 protein expression (HFSS + si-Piezo1 vs. HFSS + si-NC). Calpain-1 activity in bEnd.3 cells from different groups was analyzed using a commercial kit (Fig. 3G). Regardless of normoxia or hypoxia, HFSS-induced cells exhibited increased Calpain-1 activity (HFSS + si-NC vs. si-NC; P<0.001), while this activity was reduced following Piezo1 silencing (HFSS + si-Piezo1 vs. HFSS + si-NC; P<0.001). Western blot analysis indicated that HFSS treatment increased the SBDP/Spectrin ratio in bEnd.3 cells under both normoxic and hypoxic conditions (HFSS + si-NC vs. si-NC; P<0.001), an effect that was

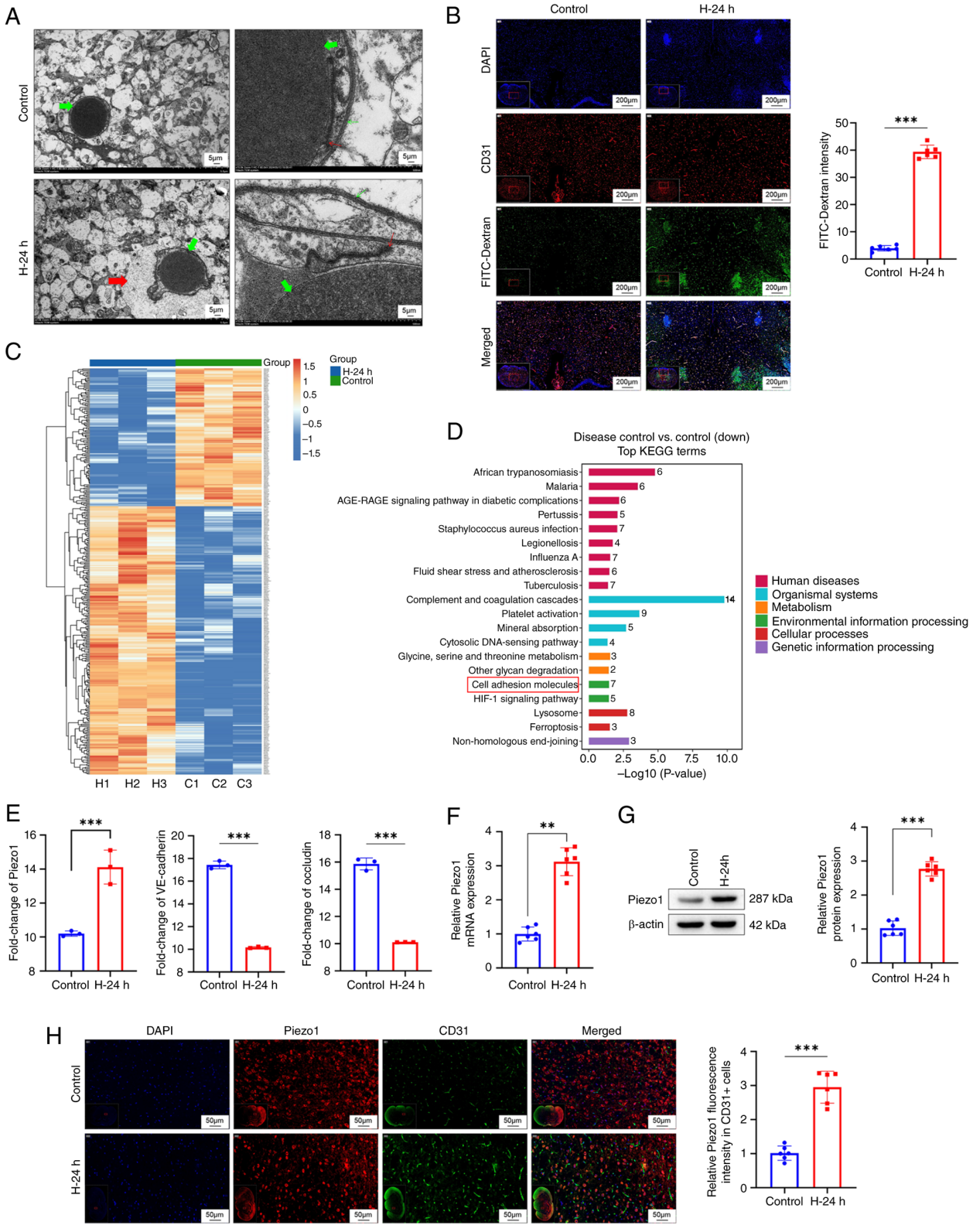


Figure 2. Hypobaric hypoxia exposure resulted in increased microvascular permeability and impaired tight junctions and Piezo1 expression within microvascular endothelial cells in the brains of mice. (A) As observed in transmission electron microscopy images, mice exposed to hypobaric hypoxia conditions for 24 h showed impaired tight junctions in brain microvessels (n=6). (B) FITC-Dextran leakage assay showed increased microvascular permeability in the brains of mice after hypobaric hypoxia exposure for 24 h. CD31 immunofluorescence staining was applied to localize brain microvascular endothelial cells (n=6). (C) Heatmap of differentially expressed proteins. (D) KEGG enrichment analysis indicated that the differentially expressed proteins might be associated with cell adhesion molecules. (E) Based on proteomics analysis, Piezo1 expression was elevated, while VE-cadherin and occludin expression were decreased in brain microvascular endothelial cells of mice subjected to hypobaric hypoxia exposure for 24 h (n=3). (F) Reverse transcription-quantitative PCR and (G) western blot showed increased Piezo1 mRNA and protein expression in brain microvascular endothelial cells of mice exposed to hypobaric hypoxia conditions for 24 h (n=6). (H) Immunofluorescence staining showed increased Piezo1 expression in brain microvascular endothelial cells of mice subjected to hypobaric hypoxia treatment for 24 h (n=6). **P<0.01 and ***P<0.001 vs. control group. Statistical tests were performed using Student's t-test. Error bars represented SD, reflecting the dispersion of individual observations around the group mean. KEGG, Kyoto Encyclopedia of Genes and Genomes; VE-cadherin, vascular endothelial cadherin; DC, disease control; C, control.

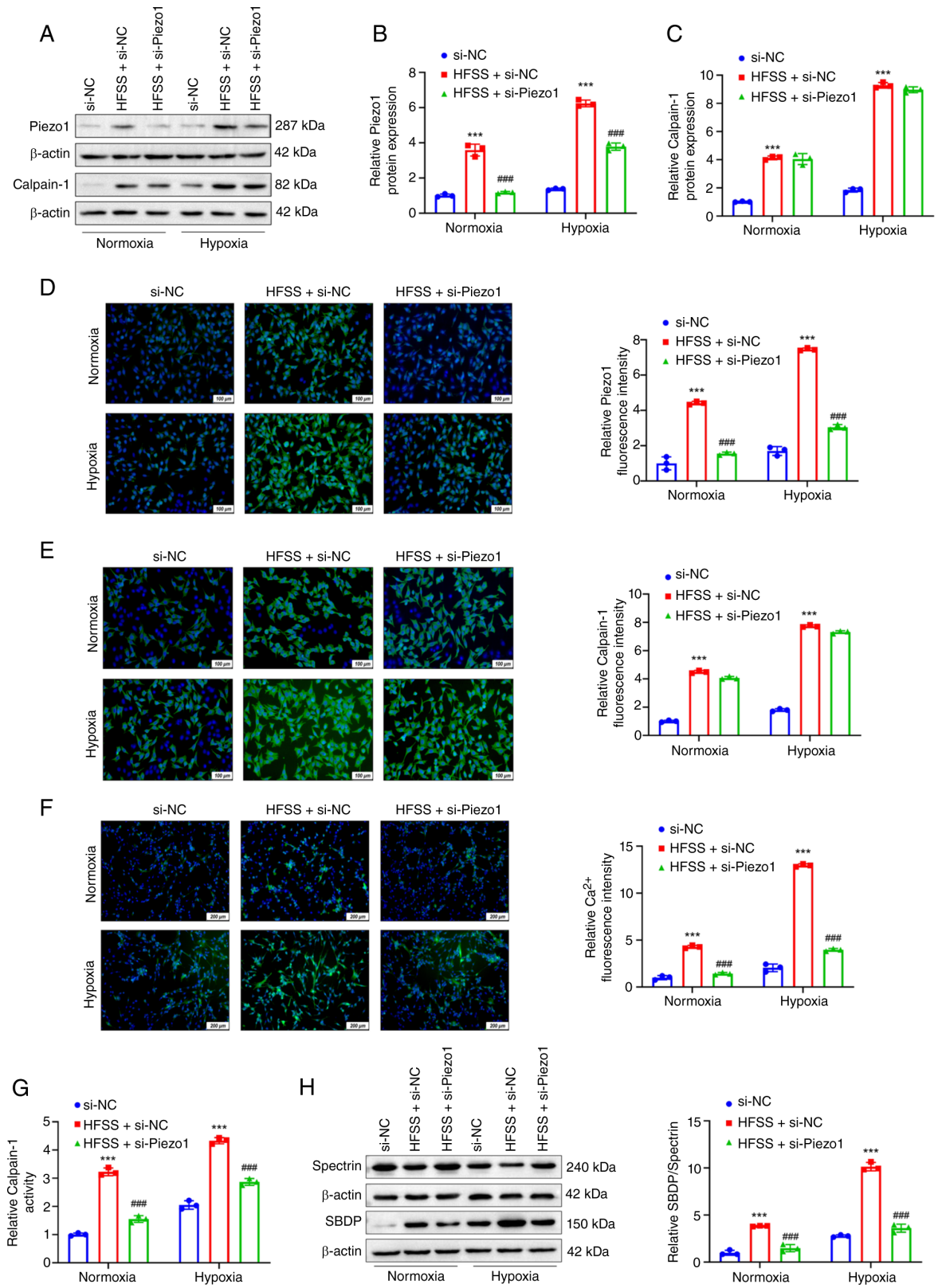


Figure 3. Piezo1 silencing reduced intracellular Ca^{2+} levels and Calpain-1 activity in HFSS- and hypoxia-induced bEnd.3 cells. (A-C) Western blot showed decreased Piezo1 protein expression in HFSS-induced bEnd.3 cells under normoxia and hypoxia conditions, while Piezo1 silencing had no notable influence on Calpain-1 protein expression in HFSS-induced bEnd.3 cells (n=3). (D and E) Immunofluorescence staining showed that Piezo1 siRNA transfection reduced (D) Piezo1 protein expression in HFSS-induced bEnd.3 cells under normoxia and hypoxia conditions but had no notable effect on (E) Calpain-1 protein expression (n=3). (F) Fluo4-AM fluorescent probe detection indicated that Piezo1 silencing decreased intracellular Ca^{2+} levels in HFSS-induced bEnd.3 cells under normoxia and hypoxia conditions (n=3). (G) Calpain-1 activity was detected using a commercial kit. Piezo1 silencing inhibited Calpain-1 activity in HFSS-induced bEnd.3 cells under normoxia and hypoxia conditions (n=3). (H) As shown by western blot analysis, under normoxia and hypoxia conditions, HFSS treatment increased the ratio of SBDP/Spectrin protein in bEnd.3 cells, whereas Piezo1 silencing reversed this effect (n=3). ***P<0.001 vs. si-NC group. $^{###}$P<0.001 vs. HFSS + si-NC group. Statistical tests were performed using ANOVA with post-hoc Tukey's test. Error bars represented SD, reflecting the dispersion of individual observations around the group mean. HFSS, high fluid shear stress; siRNA, small interfering RNA; SBDP, spectrin breakdown products; NC, negative control.

abolished by Piezo1 silencing (HFSS + si-Piezo1 vs. HFSS + si-NC; P<0.001). These results suggest that Piezo1 silencing reduces intracellular Ca^{2+} levels and Calpain-1 activity in HFSS-treated bEnd.3 cells under hypoxic conditions. Given that Calpain-1 activity depends on calcium influx, the findings indicate that Piezo1 silencing may attenuate Calpain-1 activity in HFSS-treated bEnd.3 cells by reducing calcium influx.

Silencing Piezo1 alleviated the HFSS- and hypoxia-induced tight junction dysfunction in microvascular endothelial cells. Cell viability of bEnd.3 cells was assessed using the CCK-8 assay, revealing that HFSS treatment significantly reduced cell viability under both normoxic and hypoxic conditions (HFSS + si-NC vs. si-NC group; P<0.001). Following Piezo1 silencing, increased cell viability was observed in HFSS-treated cells under both conditions (HFSS + si-Piezo1 vs. HFSS + si-NC group; P<0.001) (Fig. 4A). Subsequently, cell membrane permeability was evaluated through TEER measurement (Fig. 4B), and the expression of tight junction-associated proteins, including VE-cadherin, occludin, claudin-5 and ZO-1, was examined by western blot analysis (Fig. 4C). HFSS treatment under normoxic and hypoxic conditions decreased TEER and reduced the expression of VE-cadherin, occludin, claudin-5 and ZO-1 (HFSS + si-NC vs. si-NC group; P<0.001). Conversely, Piezo1 silencing reversed these effects, leading to increased TEER and elevated expression of VE-cadherin, occludin, claudin-5 and ZO-1 in HFSS-treated cells under both conditions (HFSS + si-Piezo1 vs. HFSS + si-NC group; P<0.001). These results indicate that Piezo1 silencing alleviates HFSS- and hypoxia-induced tight junction dysfunction in microvascular endothelial cells.

Calpain-1 inhibition reduced Calpain-1 activity and enhanced tight junction expression within the HFSS- and hypoxia-induced microvascular endothelial cells. Calpain-1 inhibitor PD150606 was applied to HFSS-treated bEnd.3 cells. Under both normoxic and hypoxic conditions, HFSS treatment alone significantly increased Calpain-1 activity (HFSS vs. control group; P<0.001), whereas PD150606 treatment reversed this increase (HFSS + PD150606 vs. HFSS group; P<0.001) (Fig. 5A). Furthermore, HFSS treatment decreased bEnd.3 cell viability (HFSS vs. Control group; P<0.001), which was restored following PD150606 treatment (HFSS + PD150606 vs. HFSS group; P<0.001) (Fig. 5B). TEER measurements (Fig. 5C) and western blot analysis (Fig. 5D) demonstrated that HFSS reduced TEER and decreased the expression of VE-cadherin, occludin, claudin-5 and ZO-1 in bEnd.3 cells (HFSS vs. control group; P<0.001). These reductions were reversed by PD150606 treatment (HFSS + PD150606 vs. HFSS group; P<0.001). Collectively, these results indicate that inhibition of Calpain-1 decreases its activity and enhances tight junction expression in HFSS- and hypoxia-induced microvascular endothelial cells. Overall, the *in vitro* data suggest that Piezo1 silencing mitigates HFSS- and hypoxia-induced tight junction dysfunction by reducing Calpain-1 activity.

Piezo1-specific agonist might exacerbate the disruption of tight junctions within microvascular endothelial cells under hypoxic conditions by enhancing the calcium influx-mediated Calpain-1 activity. The classic HACE cell model was simulated by exposing bEnd.3 cells to hypoxic conditions. Yoda1, a specific agonist of Piezo1, was then applied to bEnd.3 cells. TEER measurements indicated that both hypoxia exposure (model group) and Yoda1 treatment (Yoda1 group) significantly decreased TEER in bEnd.3 cells compared with the control group (P<0.001). Notably, Yoda1 treatment further reduced TEER under hypoxic conditions (model + Yoda1 group vs. model group; P<0.001) (Fig. 6A). Western blot analysis demonstrated reductions in the protein expression of VE-cadherin, occludin and ZO-1 in bEnd.3 cells exposed to hypoxia (model group vs. control group) or treated with Yoda1 (Yoda1 group vs. control group) (P<0.001). Yoda1 treatment under hypoxia resulted in further decreases in the expression of these proteins (model + Yoda1 group vs. model group; P<0.001) (Fig. 6B-E). Intracellular Ca^{2+} levels were measured using Fluo4-AM fluorescent probe detection, revealing elevated Ca^{2+} levels in bEnd.3 cells subjected to hypoxia (model group vs. control group) or Yoda1 treatment (Yoda1 group vs. control group) (P<0.001). Under hypoxic conditions, Yoda1 further increased intracellular Ca^{2+} levels in bEnd.3 cells (model + Yoda1 group vs. model group; P<0.001) (Fig. 6F).

Calpain-1 activity was assessed using a commercial kit (Fig. 6G), and its protein expression was analyzed by western blot analysis (Fig. 6H). Both hypoxia exposure and Yoda1 treatment increased Calpain-1 activity (P<0.001) and protein expression (P<0.05) in bEnd.3 cells (model group vs. control group; Yoda1 group vs. control group). Yoda1 treatment under hypoxia further enhanced Calpain-1 activity but did not significantly alter Calpain-1 protein expression (model + Yoda1 group vs. model group) Furthermore, the SBDP/Spectrin protein ratio was higher in bEnd.3 cells exposed to hypoxia and treated with Yoda1 (model group vs. control group; Yoda1 group vs. control group; P<0.001). After Yoda1 treatment under hypoxia, the SBDP/Spectrin ratio increased further (model + Yoda1 group vs. model group; P<0.001) (Fig. 6I). These results suggest that the Piezo1-specific agonist Yoda1 exacerbates tight junction disruption in microvascular endothelial cells under hypoxic conditions by enhancing calcium influx-mediated Calpain-1 activity.

Calpain-1 inhibitor rescued the disrupted tight junctions within microvascular endothelial cells caused by Piezo1 overexpression. The experiments in this section were carried out under normoxic conditions. Piezo1 overexpression vectors were transfected into bEnd.3 cells, resulting in a significant increase in Piezo1 mRNA and protein levels (Piezo1-OE group vs. Vector group; P<0.001) (Fig. 7A and B). TEER measurements (Fig. 7C) and western blot analysis (Fig. 7D) indicated that Piezo1 overexpression significantly decreased TEER and the expression of VE-cadherin, occludin and ZO-1 proteins in bEnd.3 cells (Piezo1-OE group vs. vector group; P<0.001). By contrast, treatment with the Calpain-1 inhibitor PD151746 increased TEER and occludin protein expression in bEnd.3 cells (vector + PD151746 group vs. vector group; P<0.05), although PD151746 did not significantly affect VE-cadherin or ZO-1 protein levels (vector + PD151746 vs. vector group). Compared with the Piezo1-OE group, bEnd.3 cells in the Piezo1 + PD151746 group exhibited higher TEER and increased expression of VE-cadherin, occludin and ZO-1 proteins (P<0.001). These findings indicate that Piezo1 overexpression induces HACE-like phenotypes by reducing TEER and the expression of tight junction proteins, while PD151746 reverses these

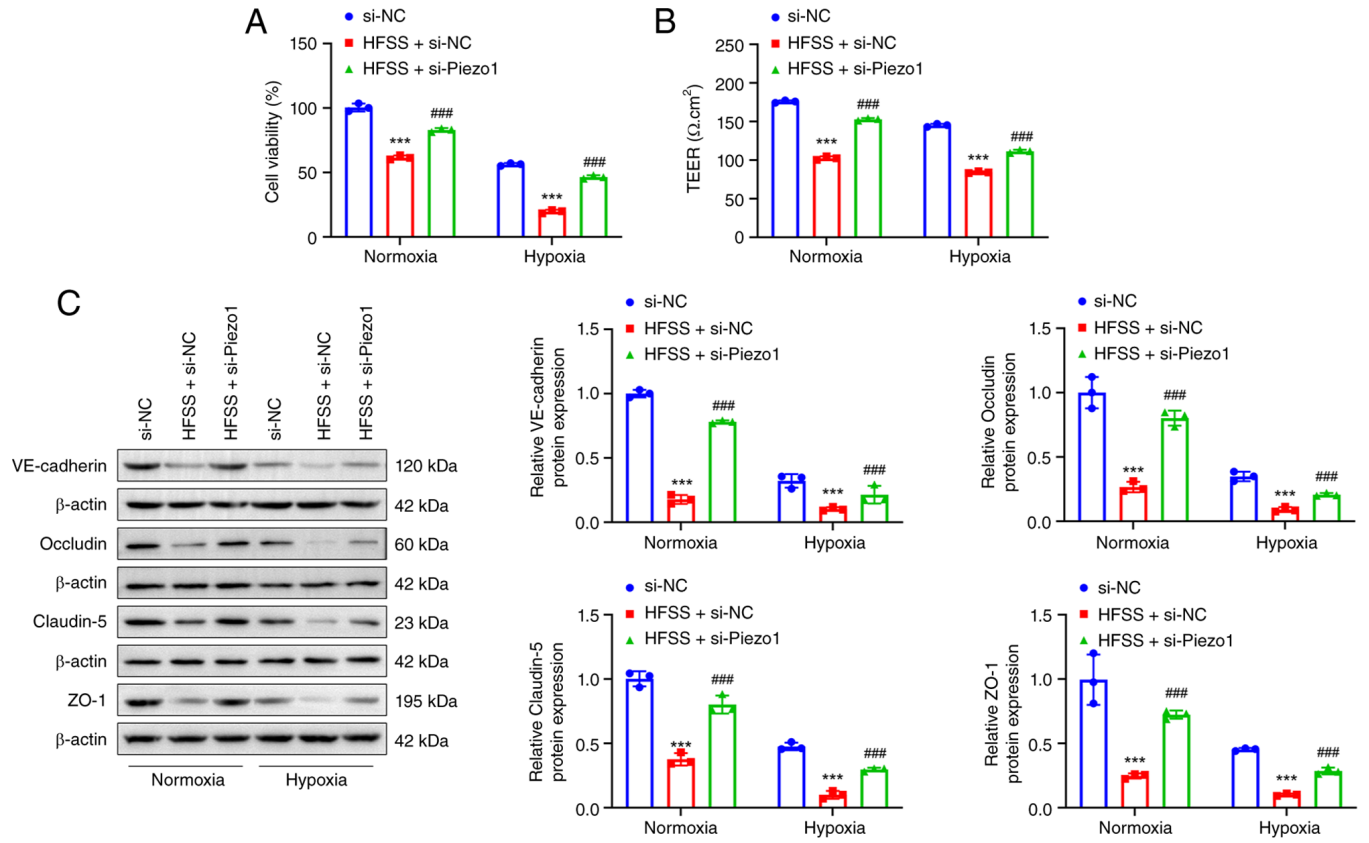


Figure 4. Silencing Piezo1 alleviates tight junction dysfunction in microvascular endothelial cells induced by HFSS and hypoxia. (A) Cell counting kit-8 assay indicated that Piezo1 silencing enhanced the viability of HFSS-treated bEnd.3 cells under normoxia and hypoxia conditions (n=3). (B) TEER measurement revealed that Piezo1 silencing attenuated cell membrane permeability of HFSS-treated bEnd.3 cells under normoxia and hypoxia conditions (n=3). (C) Western blot analysis suggested that Piezo1 silencing increased the expression of tight junction-related proteins (including VE-cadherin, occludin, claudin-5 and ZO-1) in HFSS-treated bEnd.3 cells under normoxia and hypoxia conditions (n=3). ***P<0.001 vs. si-NC group. $^{###}$P<0.001 vs. HFSS + si-NC group. Statistical tests were performed using ANOVA with post-hoc Tukey's test. Error bars represented SD, reflecting the dispersion of individual observations around the group mean. HFSS, high fluid shear stress; siRNA, small interfering RNA; NC, negative control; TEER, trans-endothelial electrical resistance; ZO-1, zonula occludens; VE-cadherin, vascular endothelial cadherin.

effects, suggesting that Piezo1 might disrupt tight junctions in microvascular endothelial cells via Calpain-1 activation.

Piezo1 effect on Calpain-1 activity was dependent on intracellular Ca^{2+} level. To investigate whether Piezo1 regulates Calpain-1 activity through Ca^{2+}, bEnd.3 cells overexpressing Piezo1 were treated with the Ca^{2+} chelator BAPTA-AM. RT-qPCR and western blot analyses indicated that Piezo1 overexpression, BAPTA-AM treatment or their combination did not significantly affect Calpain-1 mRNA or protein expression (Fig. 8A and B). However, BAPTA-AM treatment resulted in a significant reduction in Calpain-1 activity (vector + BAPTA-AM vs. vector group; P<0.001), while Piezo1 overexpression significantly elevated Calpain-1 activity (Piezo1 vs. vector group; P<0.001). Notably, the increased Calpain-1 activity induced by Piezo1 overexpression was significantly decreased following BAPTA-AM treatment (Piezo1 + BAPTA-AM vs. Piezo1-OE group; P<0.001) (Fig. 8C). Western blot analysis revealed that BAPTA-AM treatment decreased the SBDP/Spectrin ratio in bEnd.3 cells (vector + BAPTA-AM vs. vector group; P<0.001). Conversely, Piezo1 overexpression increased the SBDP/Spectrin ratio (Piezo1 vs. vector group; P<0.001), which was reversed by BAPTA-AM treatment (Piezo1 + BAPTA-AM vs. Piezo1-OE group) (P<0.001) (Fig. 8D). These data suggest that the role of Piezo1 in enhancing Calpain-1 activity is dependent on intracellular Ca^{2+} levels, indicating that increased intracellular Ca^{2+} is necessary for Calpain-1 activation.

Piezo1 knockdown could attenuate cerebral edema and microvascular permeability in mice exposed to hypobaric hypoxia. As shown in Fig. S3, the expression of Piezo1 mRNA was markedly reduced in brain microvascular endothelial cells of Piezo1 knockdown mice (the CKO-Piezo1 group), as compared with the control group (P<0.001). This suggested that Piezo1 expression was effectively down-regulated in Piezo1 knockdown mice. To further confirm the influence of Piezo1 on cerebral edema and microvascular permeability in HACE, Piezo1 knockdown mice were exposed to a hypobaric hypoxia environment. Mice subjected to hypobaric hypoxia for 24 h exhibited higher brain weight/body weight ratios and brain water content (H-24 h vs. control group; P<0.001). Piezo1 knockdown resulted in a marked decrease in brain weight/body weight ratio and brain water content in mice exposed to hypobaric hypoxia (CKO-Piezo1 + H-24 group vs. H-24 h group; P<0.001) (Fig. 9A and B).

EB staining indicated exacerbated BBB permeability in mice after 24 h of hypobaric hypoxia exposure (H-24 h vs.

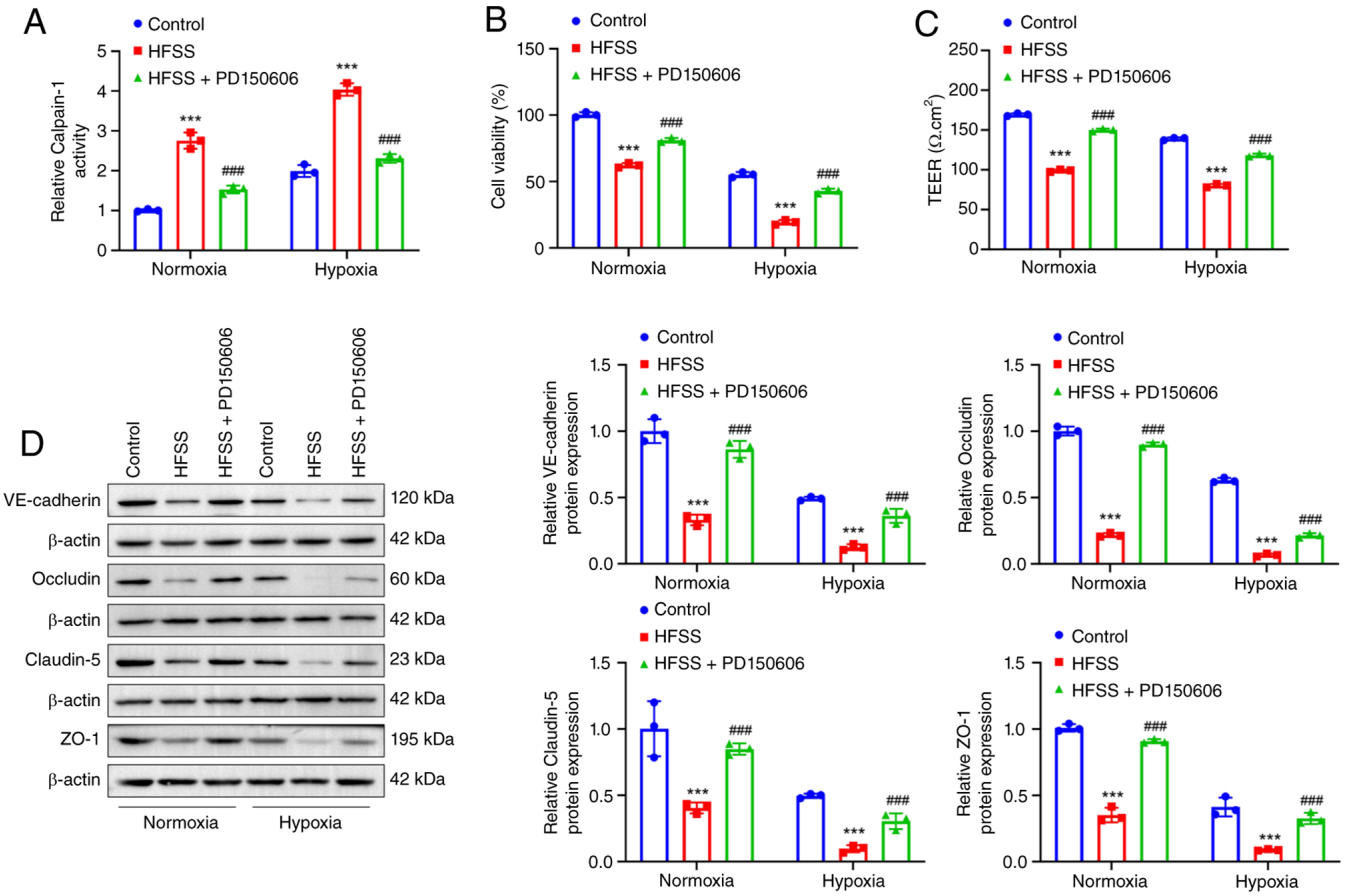


Figure 5. Blockage of Calpain-1 suppressed Calpain-1 activity and enhanced tight junctions in HFSS- and hypoxia-induced microvascular endothelial cells. (A) Under normoxia and hypoxia conditions, HFSS treatment enhanced Calpain-1 activity in bEnd.3 cells, whereas PD150606 treatment abrogated this effect (n=3). (B) Cell counting kit-8 assay showed that HFSS treatment attenuated bEnd.3 cell viability under normoxia and hypoxia conditions, which was enhanced by PD150606 treatment (n=3). (C) TEER measurement indicated that HFSS treatment increased cell membrane permeability of bEnd.3 cells under normoxia and hypoxia conditions, and this effect was counteracted by PD150606 treatment (n=3). (D) Based on western blot analysis, HFSS treatment reduced the expression of tight junction-related proteins (including VE-cadherin, occludin, claudin-5 and ZO-1) in bEnd.3 cells, which was reversed by PD150606 treatment (n=3). ***P<0.001 vs. control group. ###P<0.001 vs. HFSS group. Statistical tests were performed using ANOVA with post-hoc Tukey's test. Error bars represented SD, reflecting the dispersion of individual observations around the group mean. HFSS, high fluid shear stress; TEER, trans-endothelial electrical resistance; ZO-1, zonula occludens; VE-cadherin, vascular endothelial cadherin.

Control group; P<0.001), which was alleviated by Piezo1 knockdown (CKO-Piezo1 + H-24 group vs. H-24 h group; P<0.001) (Fig. 9C and D). H&E staining revealed marked cellular edema and nuclear condensation in the hippocampus and cerebral cortex of mice exposed to hypobaric hypoxia for 24 h (H-24 h vs. control group), with Piezo1 knockdown mitigating this damage (CKO-Piezo1 + H-24 group vs. H-24 h group) (Fig. 9E). The FITC-Dextran leakage assay demonstrated intensified microvascular permeability in the brains of mice exposed to hypobaric hypoxia for 24 h (H-24 h vs. control group; P<0.001), which was reduced by Piezo1 knockdown (CKO-Piezo1 + H-24 group vs. H-24 h group; P<0.001) (Fig. 9F). These results imply that Piezo1 knockdown effectively alleviates cerebral edema and microvascular permeability in the brains of mice exposed to hypobaric hypoxia.

Piezo1 knockdown blocked Calpain-1 activity and increased tight junction expression within brain microvascular endothelial cells of mice exposed to hypobaric hypoxia. Western blot analysis demonstrated an increase in Piezo1 and Calpain-1 protein expression in the brain microvascular endothelial cells of mice subjected to 24 h of hypobaric hypoxia treatment (H-24 h group vs. control group; P<0.001). Mice with Piezo1 knockdown exhibited decreased Piezo1 protein levels in their brain microvascular endothelial cells (CKO-Piezo1 group vs. control group; P<0.001). Additionally, Piezo1 knockdown led to a reduction in Piezo1 protein expression in the brain microvascular endothelial cells of mice experiencing hypobaric hypoxia (CKO-Piezo1 + H-24 group vs. H-24 h group) (P<0.001), while having no significant effect on Calpain-1 protein levels (CKO-Piezo1 + H-24 group vs. H-24 h group) (Fig. 10A).

Furthermore, mice exposed to hypobaric hypoxia for 24 h exhibited higher Calpain-1 activity in their brain microvascular endothelial cells (H-24 h group vs. control group; P<0.001), whereas Piezo1 knockdown significantly suppressed Calpain-1 activity (CKO-Piezo1 + H-24 group vs. H-24 h group; P<0.001) (Fig. 10B). Hypobaric hypoxia exposure for 24 h resulted in a significant reduction in the expression of VE-cadherin, occludin, claudin-5 and ZO-1 proteins in brain microvascular endothelial cells (H-24 h group vs. control group; P<0.001). Notably, Piezo1 knockdown significantly

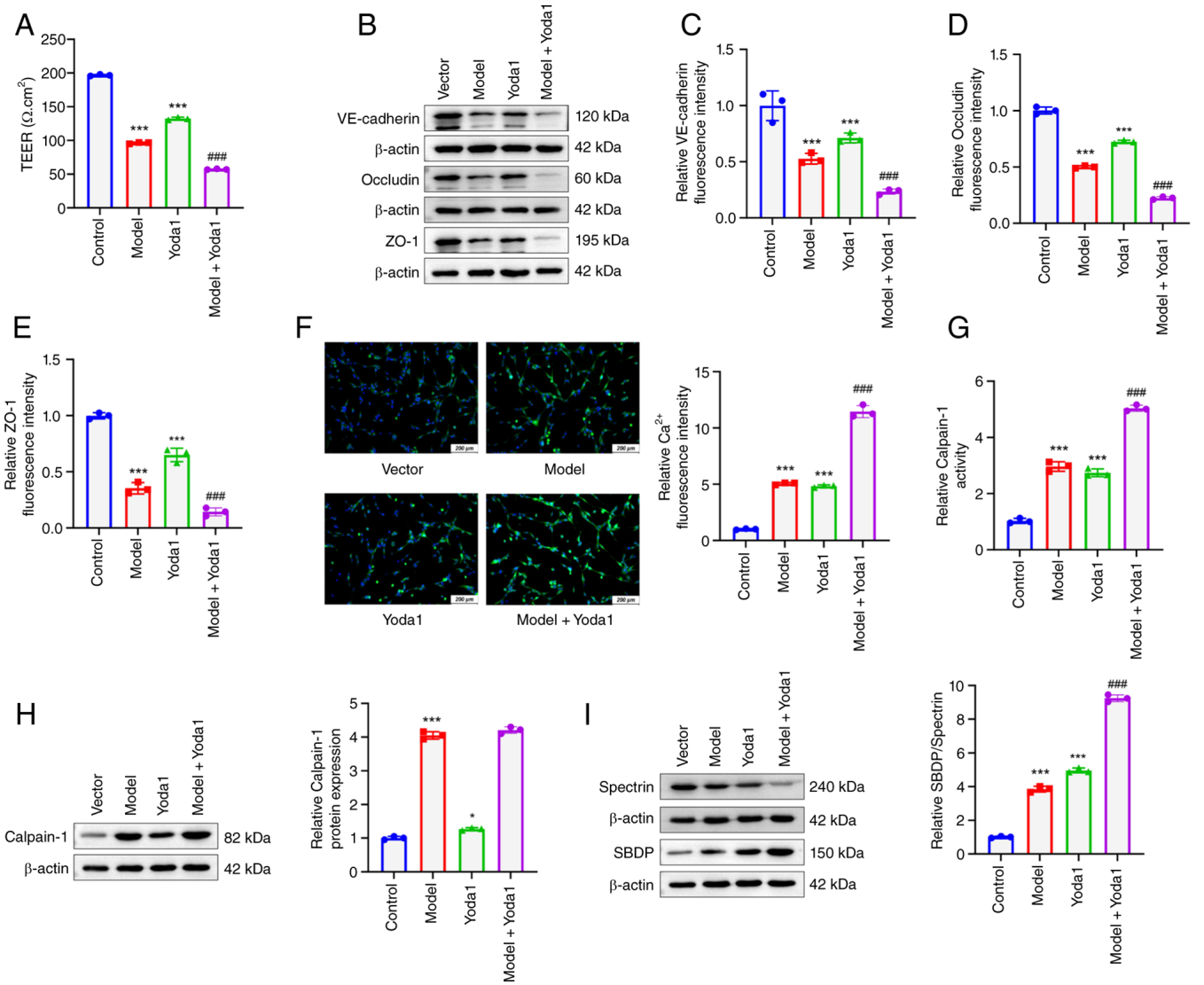


Figure 6. Piezo1-specific agonist might disrupt tight junctions within microvascular endothelial cells under hypoxia conditions via enhancing calcium influx-mediated Calpain-1 activity. (A) TEER measurement showed that Yoda1 treatment decreased TEER in bEnd.3 cells under hypoxia conditions (n=3. (B-E) Western blot analysis suggested that Yoda1 treatment reduced the expression of tight junction-related proteins, including (C) VE-cadherin, (D) occludin and (E) ZO-1) in bEnd.3 cells under hypoxia conditions (n=3). (F) Fluo4-AM fluorescent probe detection showed that Yoda1 treatment increased intracellular Ca^{2+} levels in bEnd.3 cells under hypoxia conditions (n=3). (G) Using a commercial kit, Yoda1 treatment was shown to increase Calpain-1 activity in bEnd.3 cells under hypoxia conditions (n=3). (H) Western blot analysis indicated that Yoda1 treatment had no notable effect on Calpain-1 protein expression in bEnd.3 cells under hypoxia conditions (n=3). (I) Western blot analysis revealed that Yoda1 treatment increased the ratio of SBDP/Spectrin protein in bEnd.3 cells under hypoxia conditions. (n=3). *P<0.05 and ***P<0.001 vs. control group. $^{###}$P<0.001 vs. model group. Statistical tests were performed using ANOVA with post-hoc Tukey's test. Error bars represented SD, reflecting the dispersion of individual observations around the group mean. TEER, trans-endothelial electrical resistance; ZO-1, zonula occludens; VE-cadherin, vascular endothelial cadherin.

increased the expression of these proteins (CKO-Piezo1 + H-24 group vs. H-24 h group; P<0.001) (Fig. 10C).

Therefore, Piezo1 knockdown effectively reduced Calpain-1 activity and improved tight junction integrity within brain microvascular endothelial cells of mice exposed to hypobaric hypoxia. Collectively, these findings suggest that Piezo1 knockdown may alleviate HACE by enhancing the integrity of tight junctions in brain microvascular endothelial cells through the suppression of calcium influx-mediated Calpain-1 activity.

Discussion

The present study demonstrated that Piezo1 is notably upregulated in brain microvascular endothelial cells of mice with HACE. Knockdown of Piezo1 exhibited an HACE-alleviating effect, potentially by enhancing tight junction integrity in these cells through the inhibition of calcium influx-mediated Calpain-1 activity. Although Piezo1 has received limited attention in the context of HACE, it has previously been shown to enhance cerebral edema under certain hypoxic-ischemic conditions (8). Current evidence suggests that Piezo1 knockdown may also contribute to the treatment of intracerebral hemorrhage by restoring cerebral blood flow, alleviating cerebral edema and reducing neurological deficits in mice (22,23). Endothelial cells are critical components of the BBB. Following a stroke, these cells are subjected to external pressure and tensile strain, which activate Piezo1 and exacerbate BBB disruption. Conversely, a deficiency of Piezo1 expression helps

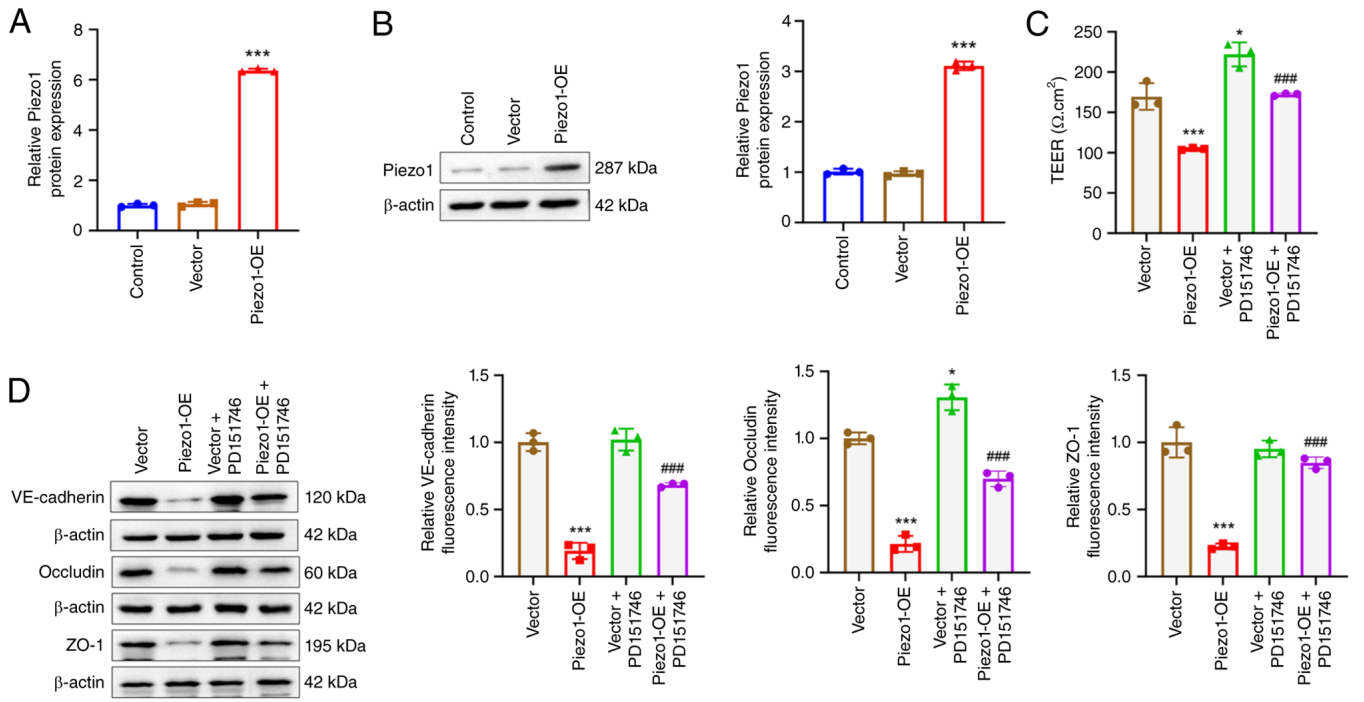


Figure 7. Piezo1 overexpression was implicated in disrupting tight junctions within microvascular endothelial cells by enhancing Calpain-1 activity under normoxic conditions. (A) Reverse transcription-quantitative PCR and (B) western blot analysis showed increased Piezo1 mRNA and protein expression in bEnd.3 cells following transfection with Piezo1 overexpression vectors under normoxic conditions (n=3). (C) TEER measurement illustrated that Calpain-1 inhibitor PD151746 treatment reversed the suppression of TEER induced by Piezo1 overexpression in bEnd.3 cells under normoxic conditions (n=3). (D) Western blot analysis suggested that Calpain-1 inhibitor PD151746 treatment abrogated the inhibitory effect of Piezo1 overexpression on the expression of VE-cadherin, occludin and ZO-1 proteins in bEnd.3 cells under normoxic conditions (n=3). *P<0.05 and ***P<0.001 vs. vector group. $^{\#\#\#}$P<0.001 vs. Piezo1-OE group. Statistical tests were performed using ANOVA with post-hoc Tukey's test. Error bars represented SD, reflecting the dispersion of individual observations around the group mean. TEER, trans-endothelial electrical resistance; ZO-1, zonula occludens; VE-cadherin, vascular endothelial cadherin.

maintain BBB integrity in both *in vitro* and *in vivo* settings (9). Additionally, Piezo1 activation by mechanical forces related to vasogenic edema can induce neuronal injury through Ca^{2+} signaling (24). In the context of vascular dementia caused by chronic cerebral hypoperfusion, treatment with a Piezo1 antagonist reduced cerebral edema in rats and preserved BBB integrity in relevant *in vitro* cell models (8). Evidence has also linked Piezo1 to BBB dysfunction and neuroinflammation resulting from mechanical stress (25). Furthermore, Piezo1 has been associated with acute vascular damage following strokes or trauma (26). Thus, Piezo1 emerges as a promising therapeutic target for interventions in central nervous system injuries (27). The present study provided key insights, revealing that Piezo1 was overexpressed in the setting of HACE and contributed to BBB damage. Specifically, the established mouse model of HACE exhibited hallmark features of cerebral edema, such as increased brain water content, altered ADC values on MRI, hippocampal and cortical damage and disrupted microvascular permeability and tight junctions (2,28,29). Notably, proteomics analysis performed in the present study, identified the overexpression of Piezo1 in brain microvascular endothelial cells of HACE-affected mice, which was further validated by immunofluorescence staining. This observation aligns with the patterns of Piezo1 expression seen in cerebral edema induced by hypoxia-ischemia (8). Notably, to the best of our knowledge, the present study represents the first demonstration of Piezo1 activation in brain microvascular endothelial cells following HACE. While Piezo1 has been implicated in other cerebrovascular diseases such as ischemic stroke, its role within the unique pathophysiological context of HACE had not been explored until now. The findings from the present study open up new avenues for HACE treatment, suggesting that targeted inhibition of Piezo1 could be a promising strategy for preventing or treating this condition.

In the present study, proteomics analysis indicated a marked reduction in VE-cadherin and occludin expression in brain microvascular endothelial cells of mice following HACE. Calpain-1, a calcium-dependent protease, acts as a downstream effector of Piezo1, being activated by elevated intracellular Ca^{2+} levels. Calpain-1 plays a role in regulating cellular functions by specifically cleaving tight junction-associated proteins, such as VE-cadherin and occluding (10,11). Cerebral hypoxia-ischemia is known to induce vascular dysfunction, and inhibition of Calpain-1 has been shown to alleviate tight junction protein loss in *in vitro* models of ischemia-reperfusion injury, as well as to mitigate BBB dysfunction and promote tight junction protein expression in mild traumatic brain injury models (30). Therefore, inhibiting Calpain-1 is proposed as a potential strategy to protect the cerebral vasculature following hypoxia-ischemia. Accordingly, the present study aimed to investigate whether Piezo1 regulates tight junctions in brain microvascular endothelial cells during HACE via Calpain-1, using *in vitro* experiments. A cell model of HACE was established by exposing bEnd.3 cells to HFSS and hypoxia. In these cells, increased intracellular Ca^{2+} levels were observed, along with elevated Calpain-1 expression and activity. Silencing

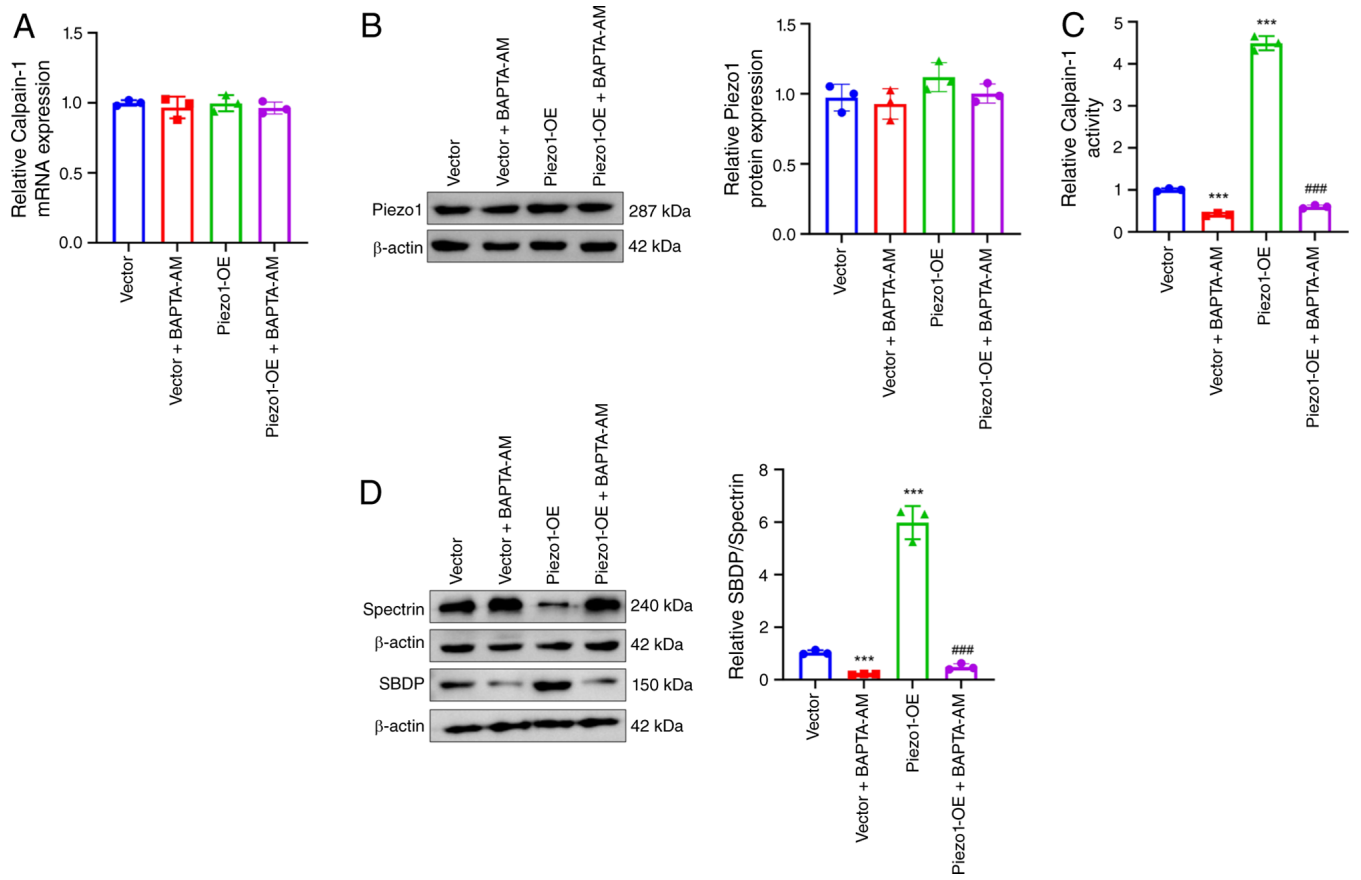


Figure 8. Piezo1 enhanced Calpain-1 activity in a manner dependent on intracellular Ca^{2+} levels. (A) Reverse transcription-quantitative PCR and (B) western blot analysis showed that Piezo1 overexpression, BAPTA-AM treatment (the mechanism of action of BAPTA-AM is to rapidly bind free Ca^{2+} within the cell with high affinity, thereby buffering calcium signaling) or a combination of both had no notable impact on the expression of Calpain-1 mRNA and protein in bEnd.3 cells (n=3). (C) Piezo1 overexpression enhanced Calpain-1 activity in bEnd.3 cells, whereas this effect was reversed by BAPTA-AM treatment (n=3). (D) Western blot analysis showed that Piezo1 overexpression increased the SBDP/Spectrin ratio in bEnd.3 cells, which was neutralized by BAPTA-AM treatment. ***P<0.001 vs. vector group. $^{###}$P<0.001 vs. Piezo1-OE group (n=3). Statistical tests were performed using ANOVA with post-hoc Tukey's test. Error bars represented SD, reflecting the dispersion of individual observations around the group mean. SBDP, spectrin breakdown products.

Piezo1 resulted in decreased intracellular Ca^{2+} levels and Calpain-1 activity in HFSS- and hypoxia-treated bEnd.3 cells; however, it did not significantly alter Calpain-1 protein expression under these conditions. Similarly, in the *in vivo* HACE mouse model, Piezo1 knockdown inhibited Calpain-1 activity but did not significantly affect Calpain-1 protein levels in the brain microvascular endothelial cells. Although Piezo1 knockdown displayed minor effects on Calpain-1 protein expression in both *in vitro* and *in vivo* experiments, these changes were not statistically significant. This suggests that Piezo1 silencing may alleviate HACE primarily by inhibiting Calpain-1 activity rather than modifying its protein expression levels. Mechanistically, Piezo1 appears to regulate Calpain-1 activity through the Ca^{2+}/Calpain tight junction axis. Specifically, Piezo1 is a mechanosensitive cation channel that detects changes in membrane tension and mediates Ca^{2+} influx, while Calpain-1 is a Ca^{2+}-dependent cysteine protease that, when activated by increased intracellular Ca^{2+}, cleaves target proteins such as VE-cadherin and occludin (11). In the present study, Piezo1 silencing reduced intracellular Ca^{2+} and inhibited Calpain-1 activity in the HACE cell model, indicating that it may block Calpain-1 activity by decreasing intracellular Ca^{2+}. Spectrin is a known substrate of Calpain-1 and is frequently used to assess Calpain-1 activity, with SBDP representing a breakdown product of Spectrin (31). In the HACE cell model, Piezo1 silencing resulted in a reduced SBDP/Spectrin ratio, while treatment with Yoda1, a Piezo1-specific agonist, increased this ratio. These findings further support the conclusion that Piezo1 silencing inhibits Calpain-1 activity within the HACE cell model by suppressing Spectrin cleavage.

Notably, the present study established a novel *in vitro* model of HACE by exposing bEnd.3 cells to a combination of HFSS and hypoxia, which represents an innovative aspect of the research. High-altitude sickness induces a compensatory increase in red blood cell count, leading to elevated blood viscosity and consequently increased shear stress in blood flow (15). This abnormal shear stress contributes to vascular endothelial dysfunction (16). Acute brain injury similarly results in elevated shear stress (5). Piezo1 is a mechanosensitive cation channel protein (32) with a unique mechanosensitive structure that enables it to detect changes in cell membrane tension, including shear stress. HFSS activates Piezo1, triggering intracellular Ca^{2+} signaling, which increases vascular permeability in endothelial cells (33-35). Accordingly, the present study aimed to investigate the role of Piezo1 in HACE using an *in vitro* model in which bEnd.3 cells were subjected to HFSS and hypoxia. While the Piezo1/intracellular Ca^{2+}/Calpain-1/tight junction disruption pathway has been studied in other neurological diseases (36,37), the present study

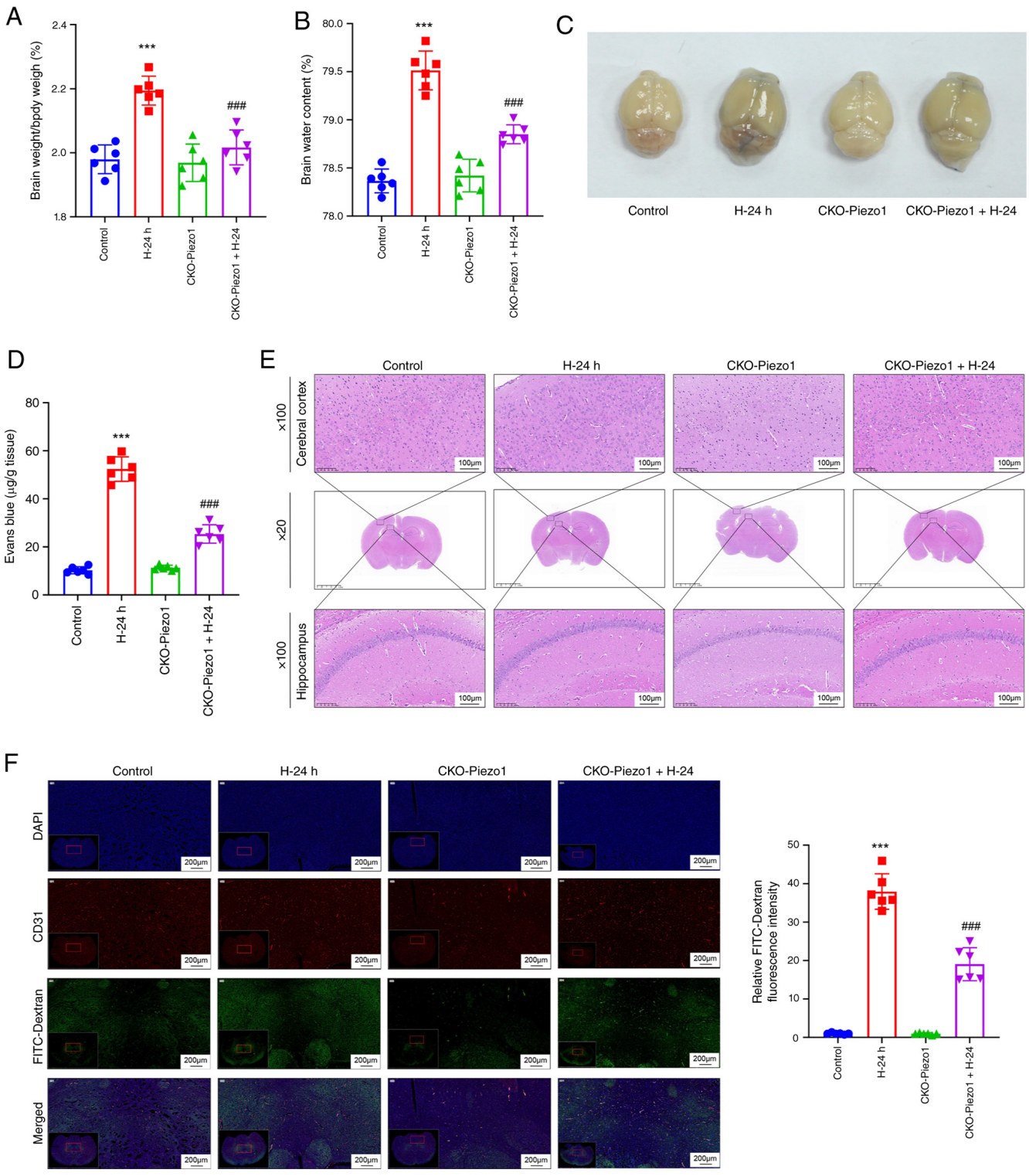


Figure 9. Piezo1 knockdown attenuated cerebral edema and microvascular permeability in the brains of mice exposed to hypobaric hypoxia. (Piezo1 knockdown decreased (A) the brain weight/body weight ratio and (B) brain water content in mice exposed to hypobaric hypoxia for 24 h (n=6). (C and D) Evans blue staining showed that Piezo1 knockdown attenuated blood-brain barrier permeability in mice exposed to hypobaric hypoxia for 24 h (n=6). (E) H&E staining suggested that Piezo1 knockdown alleviated cellular edema and nuclear condensation in the hippocampus and cerebral cortex of mice exposed to hypobaric hypoxia for 24 h (n=6). (F) FITC-Dextran leakage assay revealed that Piezo1 knockdown attenuated microvascular permeability in the brains of mice exposed to hypobaric hypoxia for 24 h (n=6). ***P<0.001 vs. control group. $^{###}$P<0.001 vs. H-24 h group. Statistical tests were performed using ANOVA with post-hoc Tukey's test. Error bars represented SD, reflecting the dispersion of individual observations around the group mean. H-24 h, hypoxia for 24 h; CKO, conditional knockout.

provides the first evidence that HFSS activates this pathway in the context of HACE. Moreover, a classic HACE model without HFSS stimulation was established in the present study to assess the effects of a Piezo1 agonist, Piezo1 overexpression and a Calpain-1-specific inhibitor on tight junctions in bEnd.3 cells. The results indicated that Piezo1 may disrupt tight junctions

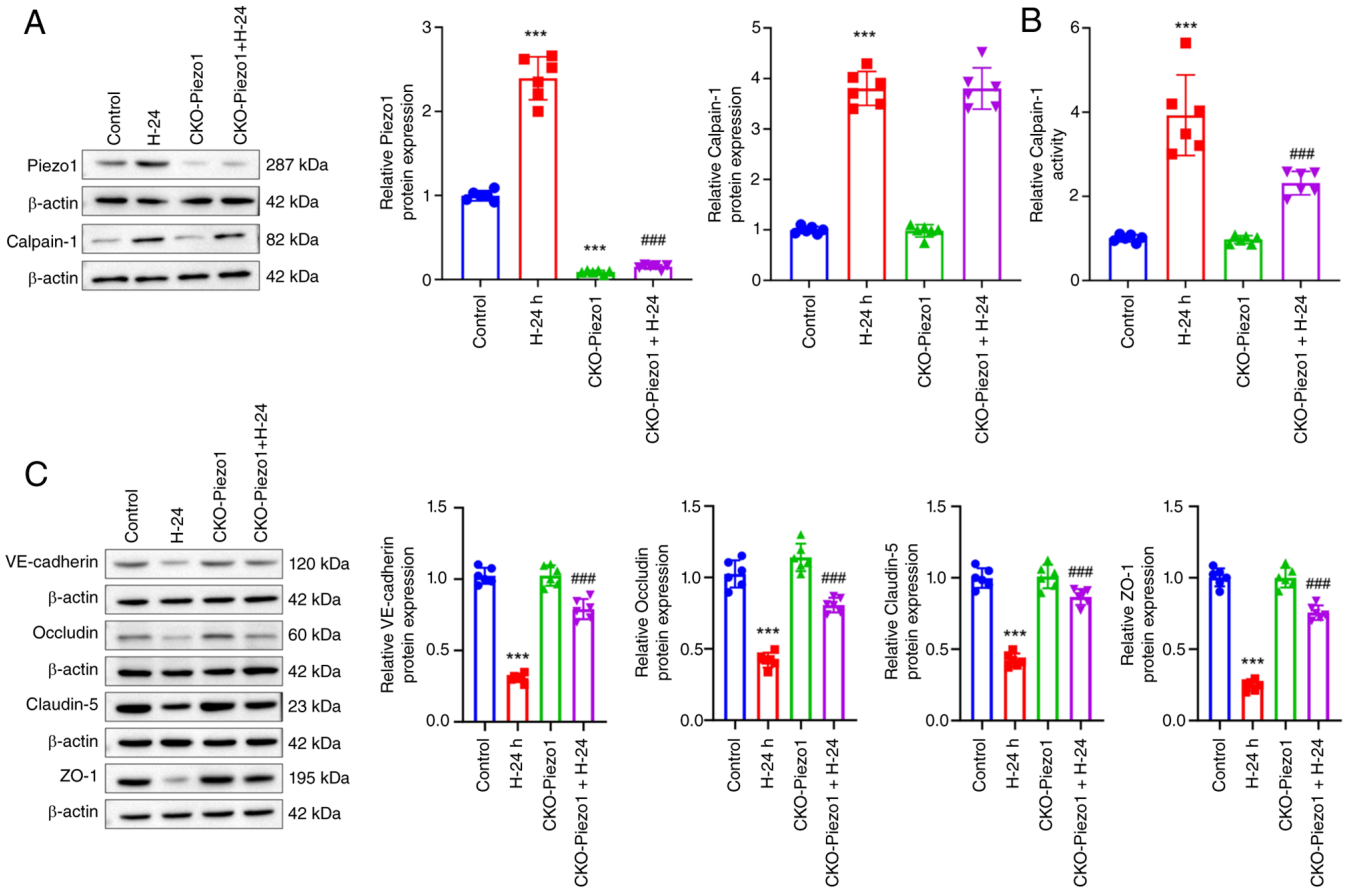


Figure 10. Piezo1 knockdown suppressed Calpain-1 activity and improved tight junctions within brain microvascular endothelial cells of mice exposed to hypobaric hypoxia. (A) Western blot analysis indicated that Piezo1 knockdown downregulated Piezo1 protein in brain microvascular endothelial cells of mice subjected to hypobaric hypoxia treatment for 24 h but had no notable effect on Calpain-1 expression (n=6). (B) Piezo1 knockdown inhibited Calpain-1 activity in brain microvascular endothelial cells of mice exposed to hypobaric hypoxia for 24 h (n=6). (C) As evidenced by western blot analysis, Piezo1 knockdown upregulated tight junction-related proteins (including VE-cadherin, occludin, claudin-5 and ZO-1) in brain microvascular endothelial cells of mice exposed to hypobaric hypoxia for 24 h (n=6). ***P<0.001 vs. control group. $^{###}$P<0.001 vs. H-24 h group. Statistical tests were performed using ANOVA with post-hoc Tukey's test. Error bars represented SD, reflecting the dispersion of individual observations around the group mean. H-24 h, hypoxia for 24 h; CKO, conditional knockout; ZO-1, zonula occludens; VE-cadherin, vascular endothelial cadherin.

in bEnd.3 cells by enhancing Calpain-1 activity, which is consistent with findings from the HFSS- and hypoxia-induced HACE cell model. Notably, contrasting observations have been made in a mouse atherosclerosis model where low shear stress down-regulates Piezo1 expression in arterial vessels, thereby promoting plaque formation. By contrast, high shear stress up-regulates Piezo1 and exerts an anti-atherosclerotic effect (38). In the present study, however, high expression of Piezo1 was shown to promote the progression of HACE in mice. This discrepancy may be attributed to the differences between brain microvascular endothelial cells and arterial endothelial cells. Consequently, Piezo1 appears to exert distinct roles in various types of vascular endothelial cells and in brain injury arising from different etiologies.

The integrity of vascular endothelial cell barriers within the central nervous system constitutes the BBB (39). As a critical measure for assessing endothelial barrier function (40), TEER was employed to evaluate the endothelial barrier integrity of bEnd.3 cells exposed to HFSS and hypoxic conditions. Under these adverse conditions, silencing Piezo1 markedly improved the impaired endothelial barrier integrity. Tight junctions in brain microvascular endothelial cells are maintained by proteins such as VE-cadherin, occludin, claudin-5 and ZO-1 (41). Piezo1 silencing promotes VE-cadherin expression in endothelial cells (42) and improves cognitive function in mice after cerebral infarction, likely by preserving ZO-1 and occludin expression (43). In the present study, Piezo1 silencing enhanced tight junction integrity in bEnd.3 cells under HFSS and hypoxia, as evidenced by increased expression of VE-cadherin, occludin, claudin-5 and ZO-1 proteins. Similarly, treatment with the calpain-1 inhibitor PD150606 also increased TEER and the expression of these tight junction proteins in HFSS- and hypoxia-induced bEnd.3 cells. These findings suggest that Piezo1 silencing protects BBB integrity in HACE by preserving tight junctions in brain microvascular endothelial cells through the inhibition of calpain-1 activity. Further *in vivo* experiments demonstrated that Piezo1 knockdown alleviated cerebral edema, protected against hippocampal and cortical damage, maintained BBB integrity and tight junctions and suppressed Calpain-1 activity without significantly affecting Calpain-1 protein expression in mice with HACE. Collectively, these results indicate that Piezo1 knockdown mitigates HACE by maintaining tight junctions in brain microvascular endothelial cells via the inhibition of

calcium influx-mediated Calpain-1 activity. Thus, targeted inhibition of Piezo1 may represent a potential therapeutic strategy for HACE.

Beyond alterations in endothelial cells, HACE involves various cell types within the neurovascular unit, including swelling of astrocytic endfeet and activation of microglia, which are critical contributors to BBB damage (44,45). Notably, Piezo1 has been implicated in microglial activation in central nervous system disorders (46). Therefore, investigating the effects of Piezo1 on astrocytic endfeet and microglia in the context of HACE represents an important avenue for future research.

The present study has several limitations. First, bEnd.3 cells were treated with HFSS to simulate blood FSS under high-altitude conditions. However, high-altitude hypoxia may also alter hemodynamics by increasing reverse shear stress (47). Developing relevant *in vitro* models can facilitate a more comprehensive understanding of the pathophysiological mechanisms underlying HACE. Second, to provide stronger evidence for the direct regulation of BBB dysfunction during HACE, it would be beneficial to perform *in vivo* experiments utilizing Piezo1 overexpression or pharmacological activation. Third, while various methods have been employed to quantitatively assess the BBB, including EB staining, FITC-dextran assay, brain tissue water content and ADC values from cranial MRI, employing additional BBB assessment techniques and quantitative analysis will provide a more thorough understanding of changes in BBB permeability. Unfortunately, current laboratory constraints precluded these experiments, which will be a priority for future investigations.

In conclusion, the present study established a mouse model of HACE and explored the impact of Piezo1 on HACE. The findings indicated that Piezo1 knockdown alleviated HACE, resulting in reduced brain water content, mitigated BBB disruption, attenuated damage in the hippocampus and cerebral cortex and maintained tight junctions in brain microvascular endothelial cells. Through *in vitro* mechanistic research, Piezo1 silencing demonstrated a HACE-alleviating effect, likely by enhancing tight junctions in brain microvascular endothelial cells via blocking calcium influx-mediated Calpain-1 activity. These discoveries illustrate that the targeted inhibition of Piezo1 may serve as a promising approach for HACE therapy.

Acknowledgements

Not applicable.

Funding

The present study was supported by the Guided Project of the Health and Wellness Commission of Qinghai Province (grant no. 2025-wjzdx-70) and the Qinghai Scholar Program of the People's Government of Qinghai Province [grant no. QZ (2024) 19].

Availability of data and materials

The mass spectrometry proteomics data generated in the present study may be found in the China National Center for Bioinformation database (https://ngdc.cncb.ac.cn/omix/release/OMIX020321; data retrieval number: OMIX020321). All other data generated in the present study may be requested from the corresponding author.

Authors' contributions

QZ conceptualized and designed the present study; TC provided administrative support and wrote the manuscript; DC and CY aided in the provision of study materials; DC performed the animal experiments and acquired the data, and drafted and revised the manuscript; CY contributed to the study design, performed the molecular experiments and data acquisition, and critically revised the manuscript for important intellectual content. DG, HM and SL collected and assembled the data; TC, ZX and YZ performed the data analysis and interpretation. All authors have read and approved the final version of the manuscript. QZ and TC confirm the authenticity of all the raw data.

Ethical approval and consent to participate

Animal experiments have been approved by the Animal Ethics Committee of Qinghai Provincial People's Hospital and are reported in accordance with the ARRIVE guidelines [approval no. (2023)-246].

Patient consent for publication

Not applicable.

Competing interests

The authors declare that they have no competing interests.

References

1. Gatterer H, Villafuerte FC, Ulrich S, Bhandari SS, Keyes LE and Burtscher M: Altitude illnesses. Nat Rev Dis Primers 10: 43, 2024.
2. Wang H, Zhang Q, Ma P, Huang N, Chen Y, Cheng Y and Chen J: High-altitude-induced cerebral edema in mice is alleviated by bestatin-mediated blood-brain barrier protection. J Neurophysiol 133: 1902-1915, 2025.
3. Xue Y, Wang X, Wan B, Wang D, Li M, Cheng K, Luo Q, Wang D, Lu Y and Zhu L: Caveolin-1 accelerates hypoxia-induced endothelial dysfunction in high-altitude cerebral edema. Cell Commun Signal 20: 160, 2022.
4. Xue Y, Wan B, Wang Z, Wang Z, Wang D, Yang W, Wang X and Zhu L: Hydroxychloroquine prevents high-altitude cerebral edema by inhibiting endothelial claudin-5 autophagic degradation. Curr Neuropharmacol 24: 404-418, 2026.
5. Zhao N, Liu C, Tian X, Yang J and Wang T: Acute brain injury increases pulmonary capillary permeability via sympathetic activation-mediated high fluid shear stress and destruction of the endothelial glycocalyx layer. Exp Cell Res 434: 113873, 2024.
6. Cheng X, Potenza DM, Brenna A, Ajalbert G, Yang Z and Ming XF: Aging increases hypoxia-induced endothelial permeability and blood-brain barrier dysfunction by upregulating arginase-II. Aging Dis 15: 2710-5415, 2024.
7. Jiang D, Zhao J, Zheng J, Zhao Y, Le M, Qin D, Huang Q, Huang J, Zhao Q, Wang L and Dong X: LOX-mediated ECM mechanical stress induces Piezo1 activation in hypoxic-ischemic brain damage and identification of novel inhibitor of LOX. Redox Biol 76: 103346, 2024.
8. Xu F, Xin Q, Ren M, Shi P and Wang B: Inhibition of piezo1 prevents chronic cerebral hypoperfusion-induced cognitive impairment and blood brain barrier disruption. Neurochem Int 175: 105702, 2024.

9. Fu H, Yu Y, Wang S, Xu P, Sun Y, Li J, Ge X and Pan S: Piezo1 disrupts blood-brain barrier via CaMKII/Nrf2 in ischemic stroke. Cell Mol Life Sci 82: 259, 2025.
10. Wu HY and Lynch DR: Calpain and synaptic function. Mol Neurobiol 33: 215-236, 2006.
11. Guo XW, Zhang H, Huang JQ, Wang SN, Lu Y, Cheng B, Dong SH, Wang YY, Li FS and Li YW: PIEZO1 Ion channel mediates ionizing radiation-induced pulmonary endothelial cell ferroptosis via Ca^{2+}/calpain/VE-cadherin signaling. Front Mol Biosci 8: 725274, 2021.
12. ElAli A, Doeppner TR, Zechariah A and Hermann DM: Increased blood-brain barrier permeability and brain edema after focal cerebral ischemia induced by hyperlipidemia: Role of lipid peroxidation and calpain-1/2, matrix metalloproteinase-2/9, and RhoA overactivation. Stroke 42: 3238-3244, 2011.
13. Alluri H, Grimsley M, Anasooya Shaji C, Varghese KP, Zhang SL, Peddaboina C, Robinson B, Beeram MR, Huang JH and Tharakan B: Attenuation of blood-brain barrier breakdown and hyperpermeability by calpain inhibition. J Biol Chem 291: 26958-26969, 2016.
14. Liu J, Wang YH, Li W, Liu L, Yang H, Meng P and Han YS: Structural and functional damage to the hippocampal neurovascular unit in diabetes-related depression. Neural Regen Res 14: 289-297, 2019.
15. Tremblay JC, Ainslie PN, Turner R, Gatterer H, Schlittler M, Woyke S, Regli IB, Strapazzon G, Rauch S and Siebenmann C: Endothelial function and shear stress in hypobaric hypoxia: Time course and impact of plasma volume expansion in men. Am J Physiol Heart Circ Physiol 319: H980-H994, 2020.
16. Tymko MM, Tremblay JC, Bailey DM, Green DJ and Ainslie PN: The impact of hypoxaemia on vascular function in lowlanders and high altitude indigenous populations. J Physiol 597: 5759-5776, 2019.
17. Karthika CL, Venugopal V, Sreelakshmi BJ, Krithika S, Thomas JM, Abraham M, Kartha CC, Rajavelu A and Sumi S: Oscillatory shear stress modulates Notch-mediated endothelial mesenchymal plasticity in cerebral arteriovenous malformations. Cell Mol Biol Lett 28: 22, 2023.
18. Choublier N, Taghi M, Menet MC, Le Gall M, Bruce J, Chafey P, Guillonneau F, Moreau A, Denizot C, Parmentier Y, *et al*: Exposure of human cerebral microvascular endothelial cells hCMEC/D3 to laminar shear stress induces vascular protective responses. Fluids Barriers CNS 19: 41, 2022.
19. Livak KJ and Schmittgen TD: Analysis of relative gene expression data using real-time quantitative PCR and the 2(-Delta Delta C(T)) method. Methods 25: 402-408, 2001.
20. Nicolicht-Amorim P, Delgado-Garcia LM, Nakamura TKE, Courbassier NR, Mosini AC and Porcionatto MA: Simple and efficient protocol to isolate and culture brain microvascular endothelial cells from newborn mice. Front Cell Neurosci 16: 949412, 2022.
21. Tejedor M, Cussó L, González-Nicolás MÁ, San Felipe D, Calle D, Martín-Sánchez B, Uzun B, Martín-Palumbo G, Alvarez-Sala Walther LA, Marco EM, *et al*: Recurrent intermittent hyponatremia: A new experimental model. PLoS One 21: e0341743, 2026.
22. Qi M, Liu R, Zhang F, Yao Z, Zhou ML, Jiang X and Ling S: Roles of mechanosensitive ion channel PIEZO1 in the pathogenesis of brain injury after experimental intracerebral hemorrhage. Neuropharmacology 251: 109896, 2024.
23. Qu J, Zong HF, Shan Y, Zhang SC, Guan WP, Yang Y and Zhao HL: Piezo1 suppression reduces demyelination after intracerebral hemorrhage. Neural Regen Res 18: 1750-1756, 2023.
24. Guo XW, Lu Y, Zhang H, Huang JQ and Li YW: PIEZO1 might be involved in cerebral ischemia-reperfusion injury through ferroptosis regulation: A hypothesis. Med Hypotheses 146: 110327, 2021.
25. Pirri C: PIEZO channels in mechano-inflammation: Gatekeepers of neuroimmune crosstalk. Diseases 13: 263, 2025.
26. Shi G, Tan R, Cao Y, Zheng X and Zhan R: Piezo1 in the central nervous system: Decoding the mechanical signature of neuroinflammation. J Neuroinflammation 23: 237, 2026.
27. Zhang M, Ge Y, Wang Z, Li H, Wang G, Zhang Y, Wang X, Hou H, Meng L, Wei L, *et al*: Insights into the role of the mechanosensitive Piezo1 channel and signaling mechanisms in CNS functions and diseases. Neurosci Biobehav Rev 183: 106562, 2026.
28. Shi H, Li P, Zhou H, Nie Z, Zhang J, Sui X, Guo J, Wang Y and Wang L: Dynamic cerebral blood flow changes with FOXOs stimulation are involved in neuronal damage associated with high-altitude cerebral edema in mice. Brain Res 1790: 147987, 2022.
29. Schoonman GG, Sándor PS, Nirkko AC, Lange T, Jaermann T, Dydak U, Kremer C, Ferrari MD, Boesiger P and Baumgartner RW: Hypoxia-induced acute mountain sickness is associated with intracellular cerebral edema: A 3 T magnetic resonance imaging study. J Cereb Blood Flow Metab 28: 198-206, 2008.
30. Knopp RC, Jastaniah A, Dubrovskyi O, Gaisina I, Tai L and Thatcher GRJ: Extending the calpain-cathepsin hypothesis to the neurovasculature: Protection of brain endothelial cells and mice from neurotrauma. ACS Pharmacol Transl Sci 4: 372-385, 2021.
31. Li J, Yang S and Zhu G: Postnatal calpain inhibition elicits cerebellar cell death and motor dysfunction. Oncotarget 8: 87997-88007, 2017.
32. Lei M, Wang W, Zhang H, Gong J, Cai H, Wang Z, Zhu L, Yang X, Wang S and Ma C: Piezo1 regulates stiffness-dependent DRG axon regeneration via modifying cytoskeletal dynamics. Adv Sci (Weinh) 11: e2405705, 2024.
33. Maneshi MM, Ziegler L, Sachs F, Hua SZ and Gottlieb PA: Enantiomeric Aβ peptides inhibit the fluid shear stress response of PIEZO1. Sci Rep 8: 14267, 2018.
34. Maneshi MM, Gottlieb PA and Hua SZ: A microfluidic approach for studying piezo channels. Curr Top Membr 79: 309-334, 2017.
35. Swain SM and Liddle RA: Piezo1 acts upstream of TRPV4 to induce pathological changes in endothelial cells due to shear stress. J Biol Chem 296: 100171, 2021.
36. Wang YY, Zhang H, Ma T, Lu Y, Xie HY, Wang W, Ma YH, Li GH and Li YW: Piezo1 mediates neuron oxygen-glucose deprivation/reoxygenation injury via Ca^{2+}/calpain signaling. Biochem Biophys Res Commun 513: 147-153, 2019.
37. Ma T, Wang YY, Lu Y, Feng L, Yang YT, Li GH, Li C, Chu Y, Wang W and Zhang H: Inhibition of Piezo1/Ca^{2+}/calpain signaling in the rat basal forebrain reverses sleep deprivation-induced fear memory impairments. Behav Brain Res 417: 113594, 2022.
38. Zhu Y, Wang T, Yang Y, Wang Z, Chen X, Wang L, Niu R, Sun Z, Zhang C, Luo Y, *et al*: Low shear stress exacerbates atherosclerosis by inducing the generation of neutrophil extracellular traps via Piezo1-mediated mechanosensation. Atherosclerosis 391: 117473, 2024.
39. Ayloo S, Lazo CG, Sun S, Zhang W, Cui B and Gu C: Pericyte-to-endothelial cell signaling via vitronectin-integrin regulates blood-CNS barrier. Neuron 110: 1641-1655.e6, 2022.
40. Ugodnikov A, Chebotarev O, Persson H and Simmons CA: Sensitivity and validation of porous membrane electrical cell substrate impedance spectroscopy (PM-ECIS) for measuring endothelial barrier properties. ACS Biomater Sci Eng 10: 5327-5335, 2024.
41. Katt ME, Xu ZS, Gerecht S and Searson PC: Human brain microvascular endothelial cells derived from the BC1 iPS cell line exhibit a blood-brain barrier phenotype. PLoS One 11: e0152105, 2016.
42. Pabst A, Brock N, Hardt S, Grannemann CCF, Kubiza H, Thiebes AL, Ludwig A and Babendreyer A: Mechanoresponsive ion channels Piezo1 and TRPV4 stimulate ADAM10 and ADAM17 with differential impact on endothelial migration and proliferation. Cell Commun Signal 24: 52, 2026.
43. Tang L, Xie D, Wang S, Gao C and Pan S: Piezo1 knockout improves post-stroke cognitive dysfunction by inhibiting the interleukin-6 (IL-6)/glutathione peroxidase 4 (GPX4) pathway. J Inflamm Res 17: 2257-2270, 2024.
44. Lafuente JV, Bermudez G, Camargo-Arce L and Bulnes S: Blood-brain barrier changes in high altitude. CNS Neurol Disord Drug Targets 15: 1188-1197, 2016.
45. Wang X, Chen G, Wan B, Dong Z, Xue Y, Luo Q, Wang D, Lu Y and Zhu L: NRF1-mediated microglial activation triggers high-altitude cerebral edema. J Mol Cell Biol 14: mjac036, 2022.
46. Zong B, Yu F, Zhang X, Pang Y, Zhao W, Sun P and Li L: Mechanosensitive Piezo1 channel in physiology and pathophysiology of the central nervous system. Ageing Res Rev 90: 102026, 2023.
47. Tremblay JC: Shear stress and flow-mediated dilation in the normoxic and hypoxic human. Appl Physiol Nutr Metab 44: 902, 2019.

Copyright © 2026 Cao et al. This work is licensed under a Creative Commons Attribution-NonCommercial-NoDerivatives 4.0 International (CC BY-NC-ND 4.0) License.